united nations
educational, scientific
and cultural
organization

international atomic
energy agency

the
abdus salam
international centre for theoretical physics

ICTP 40th Anniversary

SCHOOL ON SYNCHROTRON RADIATION AND APPLICATIONS
In memory of J.C. Fuggle & L. Fonda

19 April - 21 May 2004

Miramare - Trieste, Italy

1561/12

Microscopy Optics

W. Jark

Optics for x-ray microscopy

µXFA beamline and multilayer laboratory

Werner Jark

Sincrotrone Trieste
Basovizza (TS), Italy

werner.jark@elettra.trieste.it

http://www.elettra.trieste.it/experiments/beamlines/microfluo/index.html

Structure of lecture

Discussion of the technical aspects of x-ray microscopy (learn about applications in three weeks)

- Spatial resolution obtainable with different objectives based
  - on reflection
  - on diffraction
  - on refraction

W.C. Roentgen: There are no refractive lenses for x-rays!

- Refractive objectives unique to x-rays

Note: This presentation is neither historically correct as a whole nor complete for the single items. It is limited to (often newer) experiments, which can explain the concepts in the most instructive way.

Why microscopy with SR?

A) use unconventional contrast mechanisms, e.g.

- absorption edges (water window)
- dichroic response (helicity)
- coincidences …… more in 3 weeks

B) in visible: spatial resolution ≈ light wavelength

will shorter wavelength SR reveal the yet unseen?

Why x-ray microscopy?

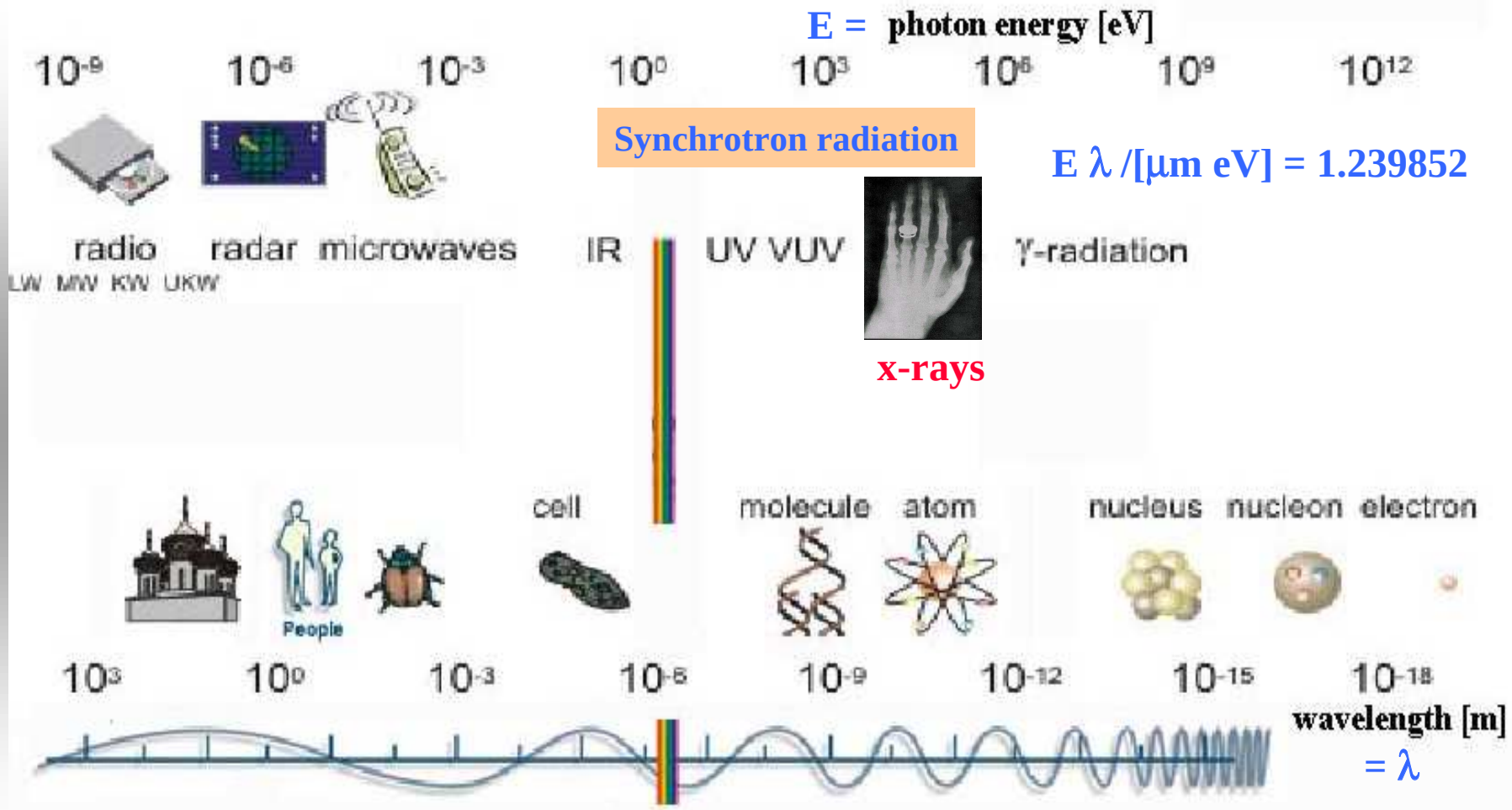

Why x-ray microscopy?

Question:

What is the ultimately possible spatial resolution?

Please note:

here we would like to see features in a single aggregate

X-ray crystallography instead reveals structures with very high spatial resolution, however, only of crystalline samples. “Lensless” or coherent x-ray diffraction imaging of intrinsically noncristalline objects promises high resolution (see elsewhere).

Microscope objectives for visible

µXFA beamline and multilayer laboratory

A) Magnifying lens

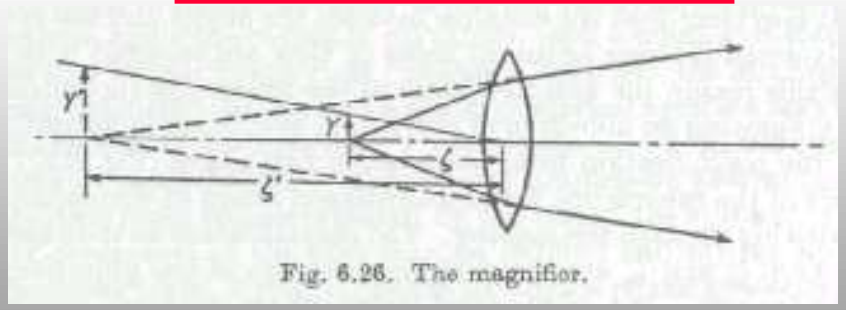

Fig. 6.26. The magnifier.

B) Microscope

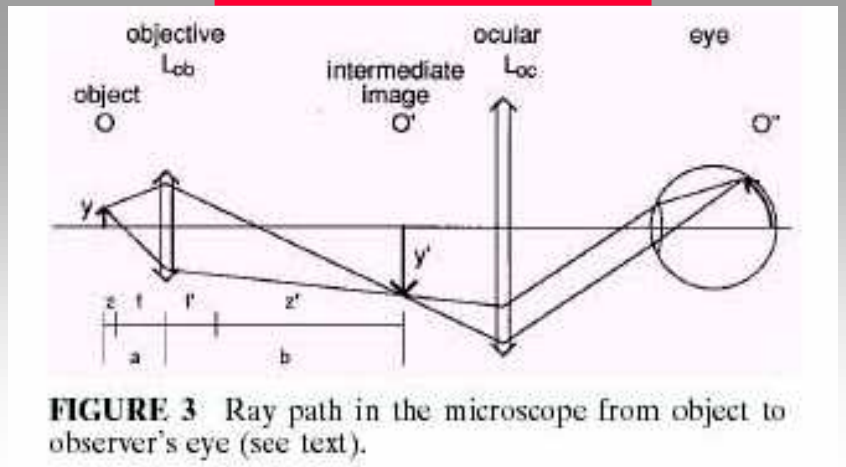

FIGURE 3 Ray path in the microscope from object to observer's eye (see text).

C) Schwarzschild objective

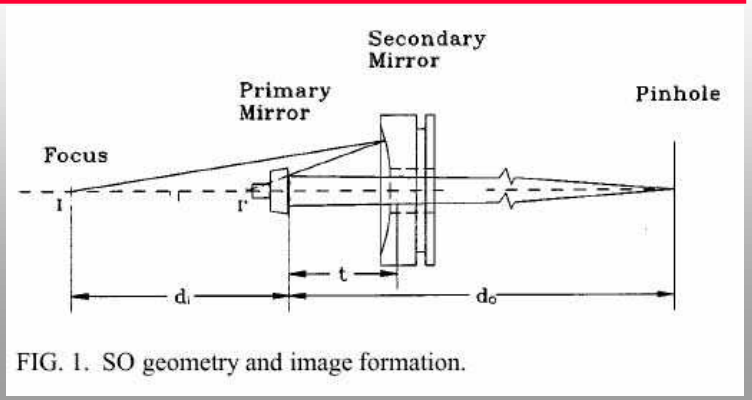

FIG. 1. SO geometry and image formation.

D) numerical aperture

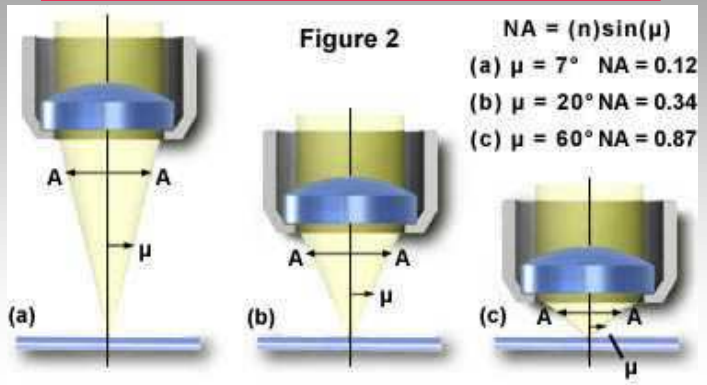

Similarities

The resolution of a microscope is given by

R = λ/(2NA) NA = numerical aperture

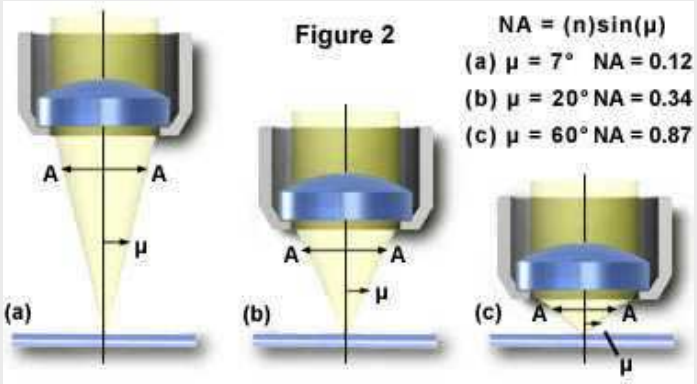

Have to focus x-rays with refraction, reflection or diffraction with largest possible NA

Characteristics of x-rays

- wavelength of order of λ=0.06 nm (E=20 keV)
- negligible absorption in air
- large variation of absorption in material
- reflected with surface mirrors only at grazing incidence Φ
  (rule of thumb for Pt coating: $E*\Phi/[keV*mrad] = 80$)
- reflected/monochromatised at lattice planes of highly regular crystal structures

Soft x-rays with 0.6 nm < λ < 30 nm (40 eV < E < 2 keV)

- significant absorption in air (vacuum required) and material
- mirrors for reflection, gratings for monochromatisation

Some basic properties

- refractive index $n = 1 - \delta + i\beta$,
  where i=sqrt(-1) and $\delta, \beta << 1$

$$\delta = \frac{r_e \lambda^2 N_e f_1}{2\pi}$$

$r_e = 2.8\ 10^{-13}$ m, N_e = no. atoms/unit volume

f_1 = tabulated atomic scattering factor (e.g. www-cxro.lbl.gov)

- in x-ray range: $\delta \propto \lambda^2$ $\beta \propto \lambda^4$
- total reflection angle $\Phi = \mathrm{sqrt}(2\delta)$
- deflection in a prism $\Delta = -2\delta/\tan(\gamma)$
- phase retardation $\Delta\psi = 2\pi l\delta/\lambda \propto \lambda$
- absorption length $1/\mu \propto \lambda^3$

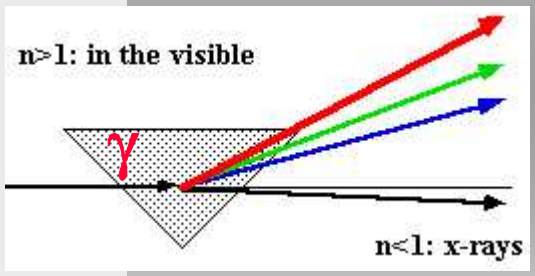

e.g. for plexiglass at λ=0.154 nm (8.05 keV): $\delta = 4.2\ 10^{-6}$ $1/\mu \approx 1.3$ mm

then $\Phi = 2.9$ mrad (0.167°) $\Delta(\gamma = 45°) = -8.4$ µrad

l =36.67 µm provide 2π phase shift

X-ray microscope schemes

µXFA beamline and multilayer laboratory

Fullfield Microscope

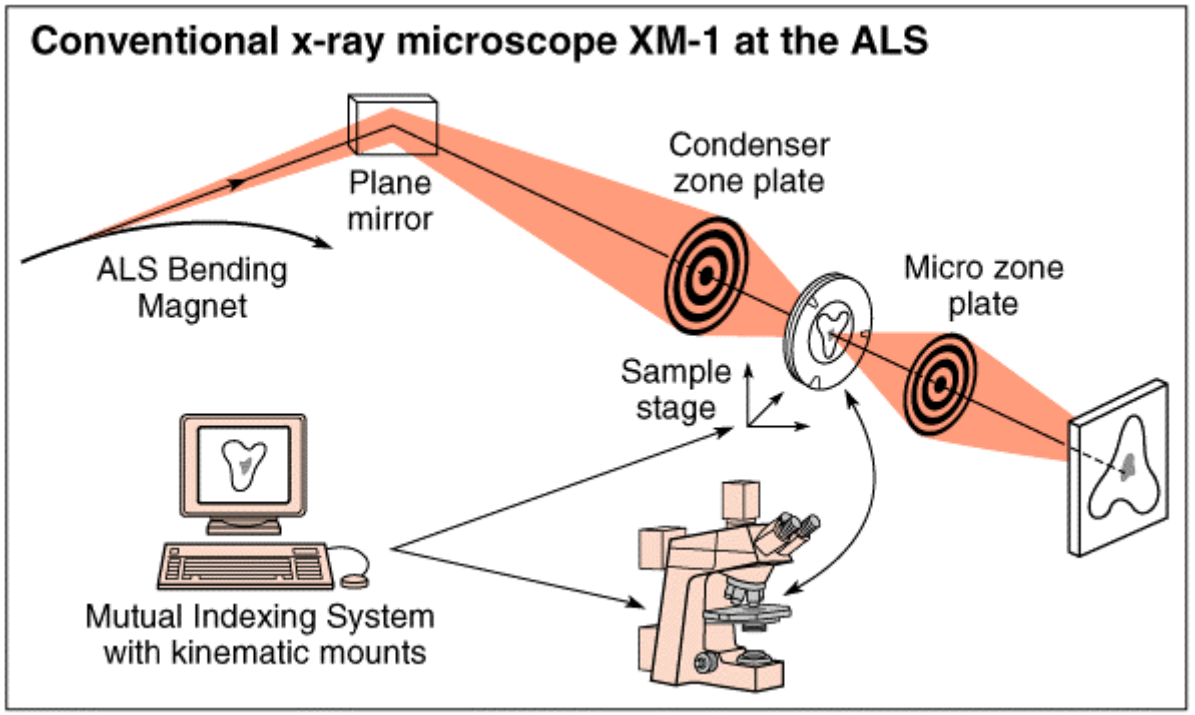

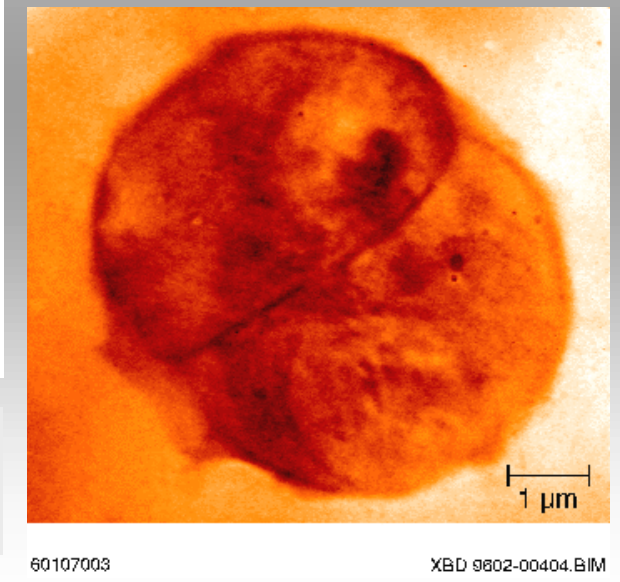

Instrumentation operated by Center for X-ray Optics at ALS, Berkeley, CA (USA)

X-ray microscope schemes

µXFA beamline and multilayer laboratory

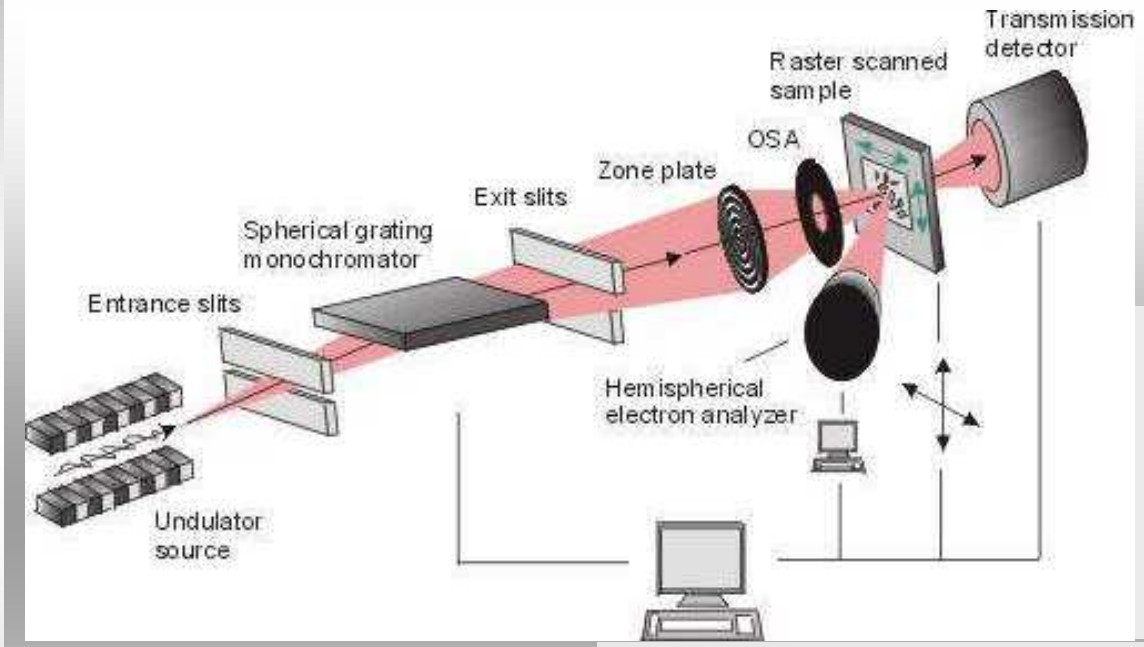

Scanning Microscope

Ni 3p and Ga 3d images (25x50 µm2) taken at (a) 25° C and (b) after annealing to 300° C, the R-Ga image in (b) manifests lateral variations in the interfacial reaction (c) C 1s image and entire spectrum measured in the C-rich spots (bottom) and in the non-defect region (top)

ESCA-microscopy beamline operated at ELETTRA

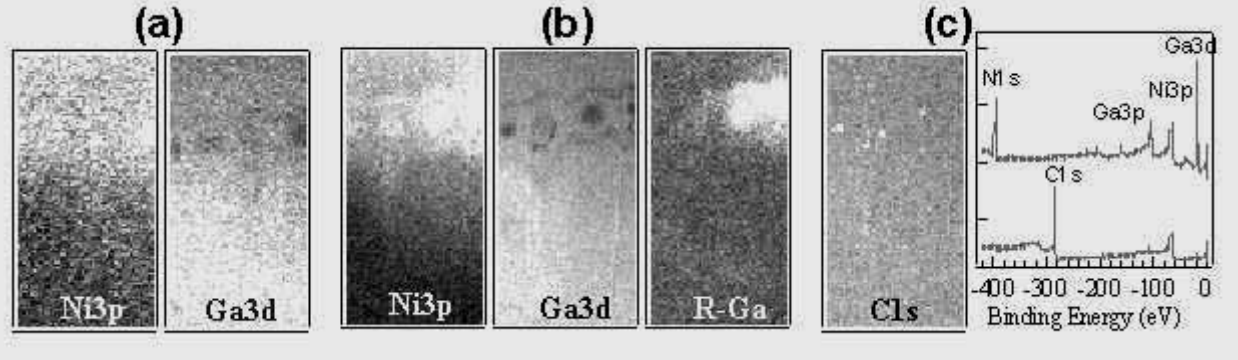

Werner Jark
ELETTRA

Spatial resolution

ultimate limit
practical limit
experimental limit

Reflection

Single bounce elliptical/parabolic capillary

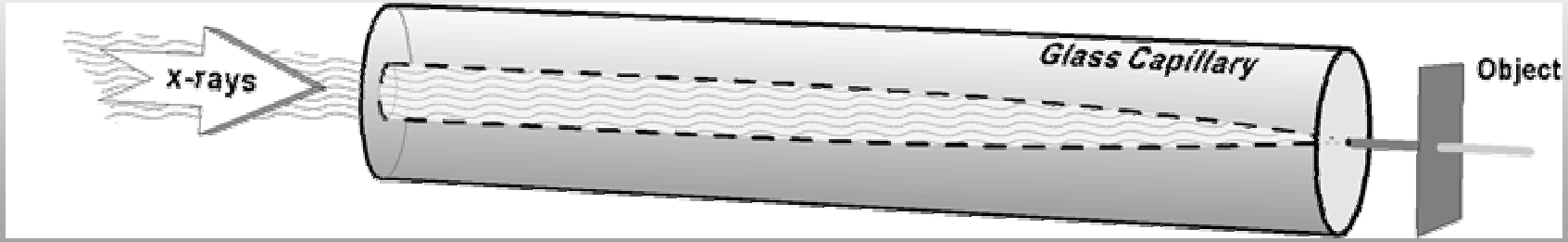

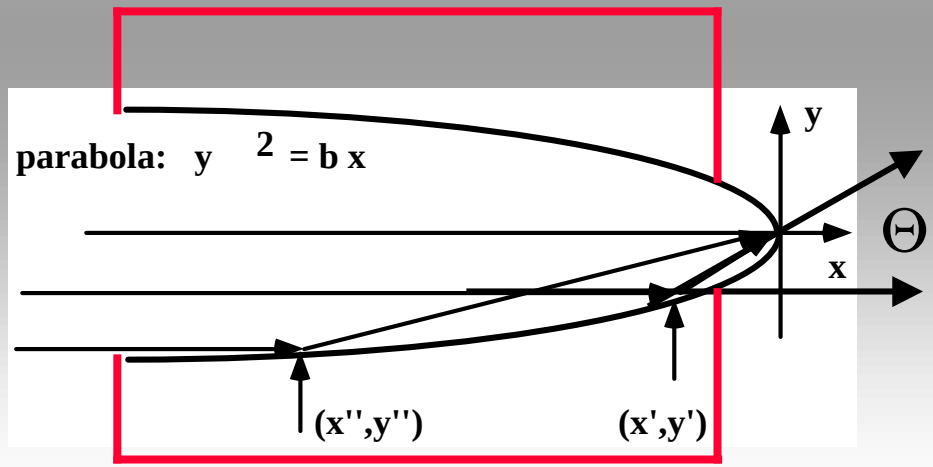

Achromatic objective

$\Theta = 2\Phi_{crit} = 2\mathrm{sqrt}(2\delta) = NA$

$R_{ult} = \lambda/(4\ \mathrm{sqrt}(2\delta)) = R_{prac}$

Spatial resolution

ultimate limit
practical limit
experimental limit

µXFA beamline and multilayer laboratory

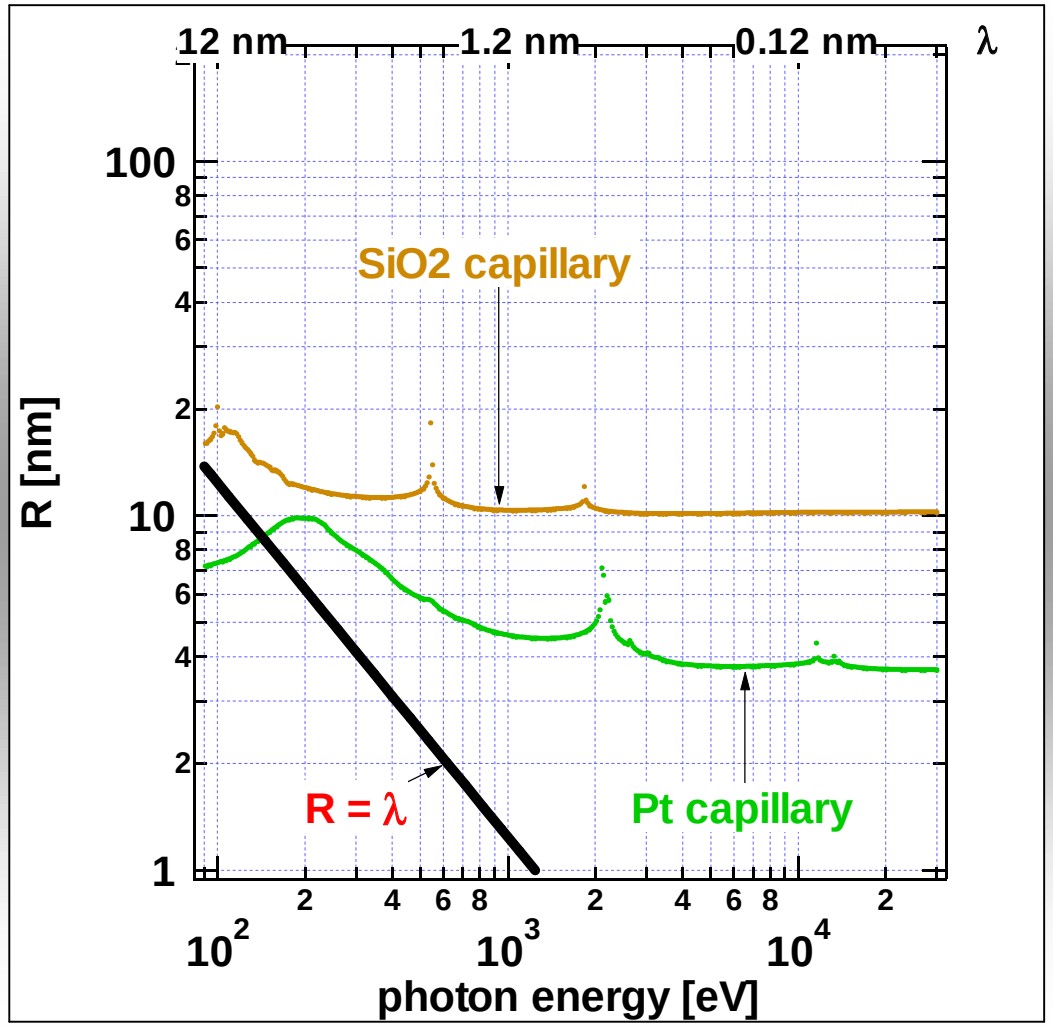

Fixed lower limit depends on Z:

R ≈ 4 nm for platinum

BUT

R_{exp} ≈ 10 µm

figure error limited (Bilderback, CHESS)

no successive figure correction possible

Spatial resolution

ultimate limit
practical limit
experimental limit

Reflection

Beam compression in multibounce capillary

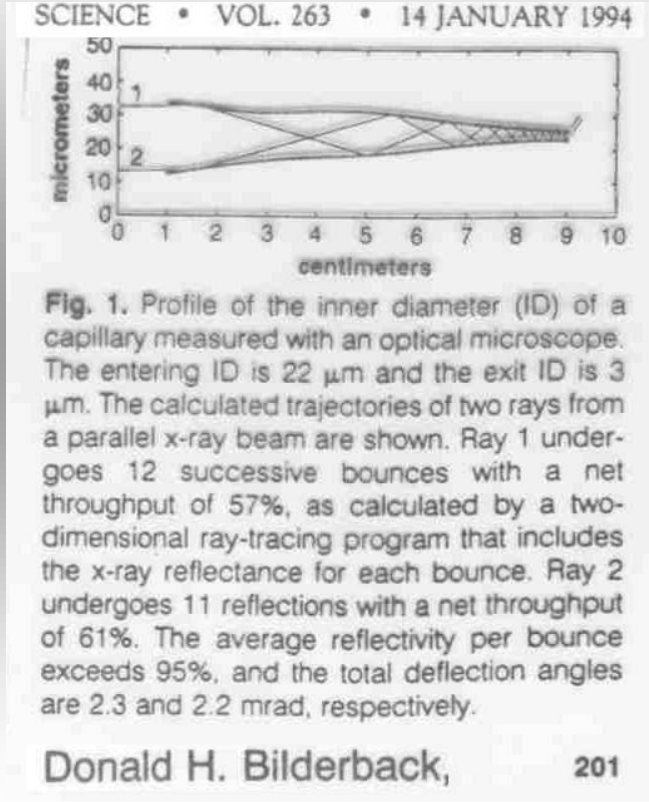

SCIENCE • VOL. 263 • 14 JANUARY 1994

Fig. 1. Profile of the inner diameter (ID) of a capillary measured with an optical microscope. The entering ID is 22 µm and the exit ID is 3 µm. The calculated trajectories of two rays from a parallel x-ray beam are shown. Ray 1 undergoes 12 successive bounces with a net throughput of 57%, as calculated by a two-dimensional ray-tracing program that includes the x-ray reflectance for each bounce. Ray 2 undergoes 11 reflections with a net throughput of 61%. The average reflectivity per bounce exceeds 95%, and the total deflection angles are 2.3 and 2.2 mrad, respectively.

Donald H. Bilderback, 201

$R_{exp} \approx 50$ nm

but

very low efficiency

better efficiency is routinely (commercially available) provided with

$R_{exp} \approx 5$ µm

Spatial resolution

ultimate limit
practical limit
experimental limit

Reflection

Crossed mirror pair (Kirkpatrick-Baez system)

Achromatic system

horizontal and vertical focusing are separated: "astigmatic" system

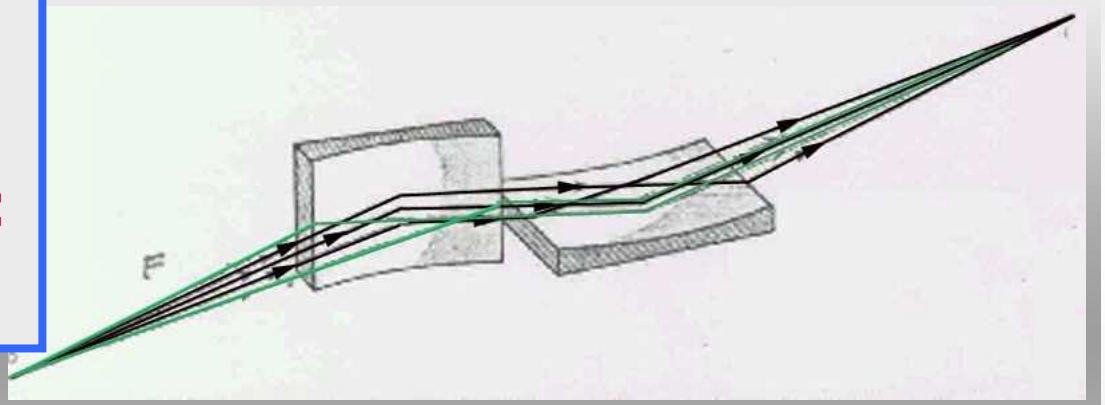

Source **Focus**

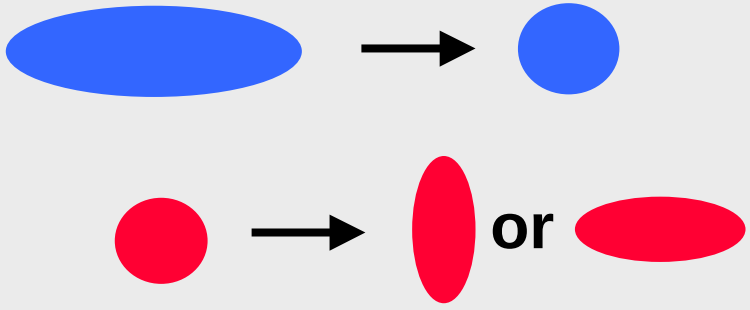

Synchrotron radiation sources

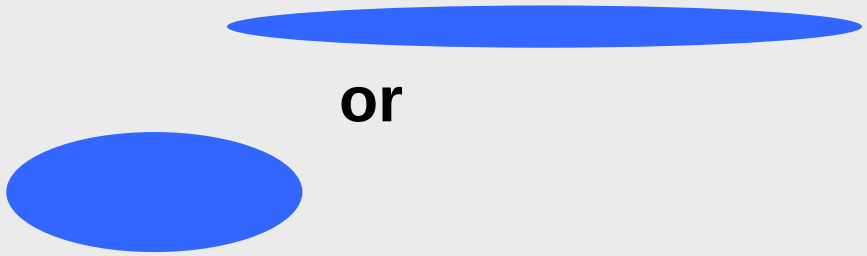

Spatial resolution

ultimate limit
practical limit
experimental limit

Reflection

Crossed mirror pair (Kirkpatrick-Baez system)

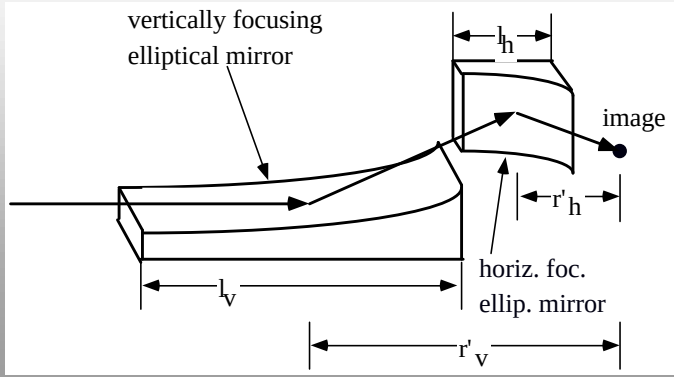

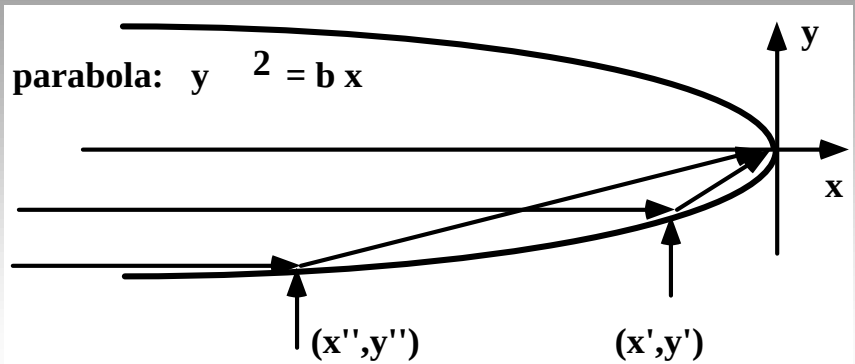

- **Ideally elliptical mirrors needed**
- **approximate as parabola** $y=(bx)^{1/2}$, $\Delta y/\Delta x = 0.5\,(b/x)^{1/2}$
- **for x=x':** $\Delta y/\Delta x\,(x') = \Phi_{crit}$
- **then** $b=(2\Phi_{crit})^2\,x'$ **and at x=x'':**

  $\Delta y/\Delta x\,(x'') = \Phi_{crit}\,(x'/x'')^{1/2}$
- **deflection angle is** $2\,\Delta y/\Delta x$
- **and convergence angle in focus** $\Delta_{(h,v),f} = 2\,NA$

  $= 2\,\Phi_{crit}[1-(x'/x'')^{1/2}]$
- **Mirror size parameter:** $q=l/r=|x''-x'|/r$

Spatial resolution

ultimate limit
practical limit
experimental limit

Reflection

Crossed mirror pair (Kirkpatrick-Baez system)

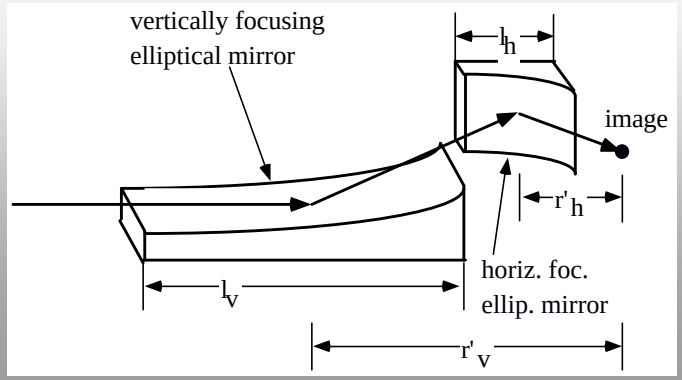

- $$NA = \Phi_{crit}\left(1 - \frac{\sqrt{2-q}}{\sqrt{2+q}}\right)$$

- **2 mirrors just touch with**
  $q_h = l_h/r'_h = l_v/r'_v = q_v = q$
  $r'_h + 0.5\ q\ r'_h = r'_v - 0.5\ q\ r'_v$
  we put $r'_v = m\ r'_h$:
  then $q = 2\ (m-1)/(m+1)$

- **at ELETTRA m=5: $q = 1.33$**
  $\Delta_{h,f} = \Delta_{v,f} = 1.1\ \Phi_{crit} = 2$ NA
- **more realistic 2 NA = Φ_{crit}**

OPERATIONAL example:
ESRF (bendable flat mirror):
f=95 mm and l=90 mm
2 NA = 0.8 Φ_{crit}
R = λ/(0.8 sqrt(2δ)) = R_{prac}
= 5 * $R_{single\ bounce\ capillary}$
exp: Φ =2.2 mrad at 20.5 keV

Spatial resolution

ultimate limit
practical limit
experimental limit

µXFA beamline and multilayer laboratory

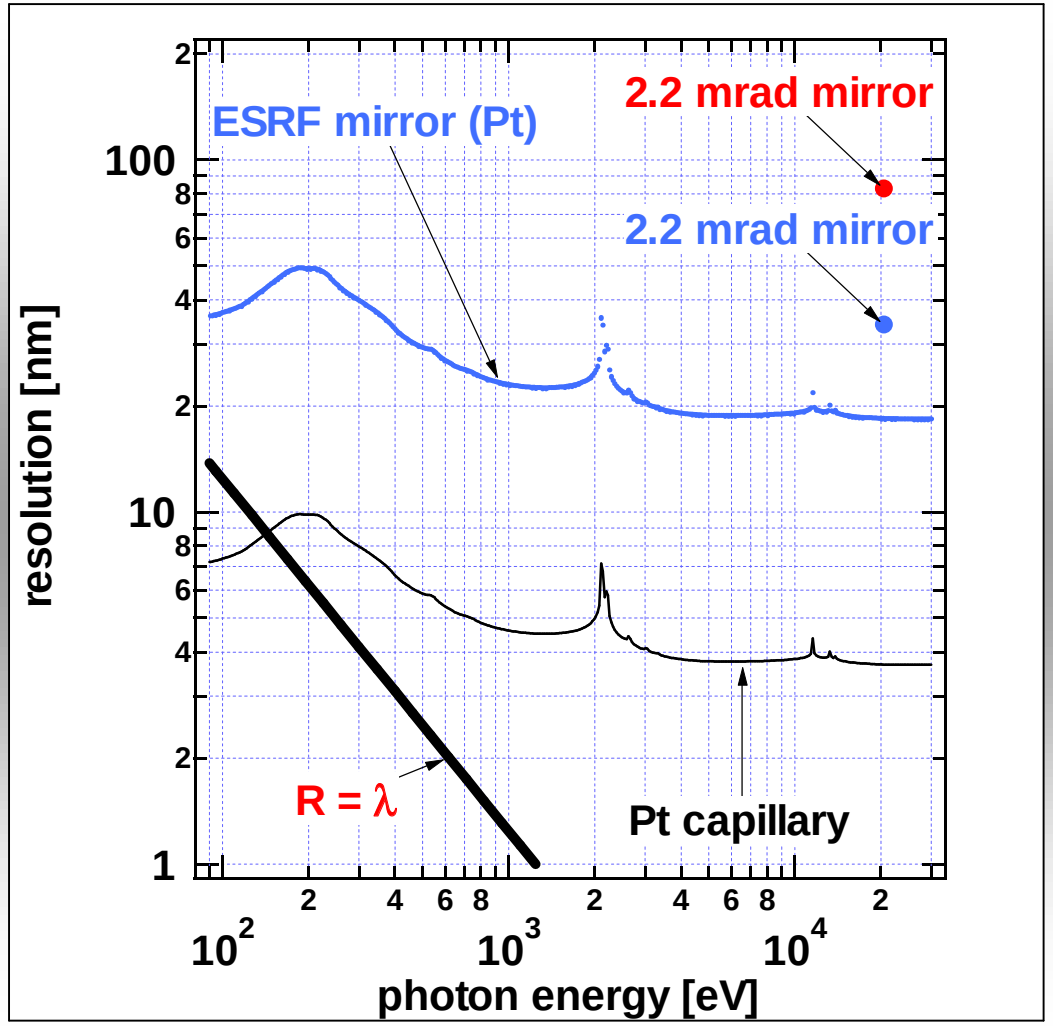

practical lower limit

$R_{prac} \approx 35$ nm for Pt

$R_{exp} \approx 83$ µm

figure error limited

(Hignette, ESRF)

Spatial resolution

ultimate limit
practical limit
experimental limit

µXFA beamline and multilayer laboratory

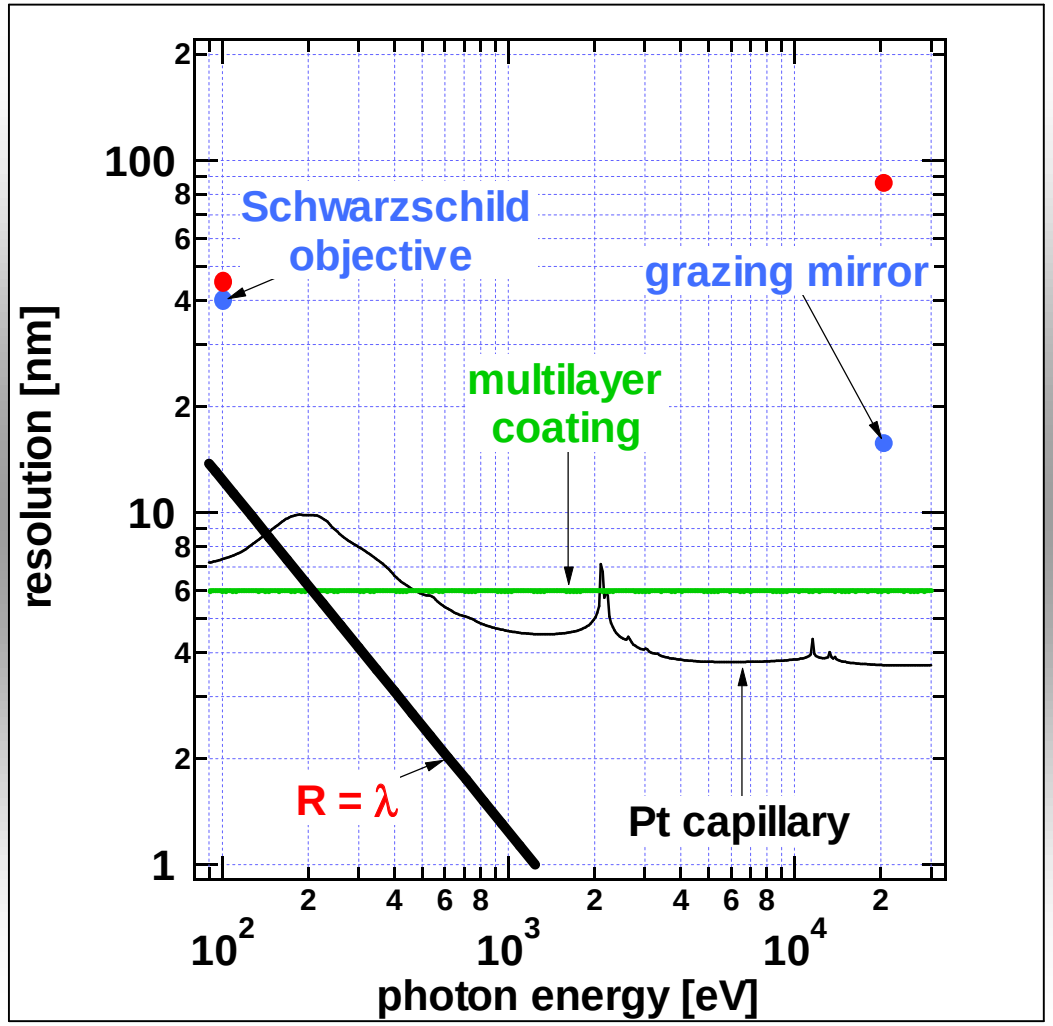

Add multilayer coating

(becomes chromatic)

R = 2 d ≈ 6 nm

ESRF (bend mirror):

f=250 mm, l=170 mm

6.5 mrad, d = 8 nm

R_{prac} ≈ 16 nm

R_{exp} ≈ 86 µm

figure error limited

(Hignette, ESRF)

Spatial resolution

ultimate limit
practical limit
experimental limit

Diffraction

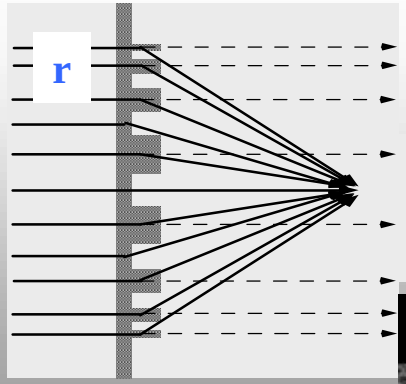

Fresnel zone plates

Highly chromatic

Zone-plates produced at INFM-TASC laboratory at ELETTRA

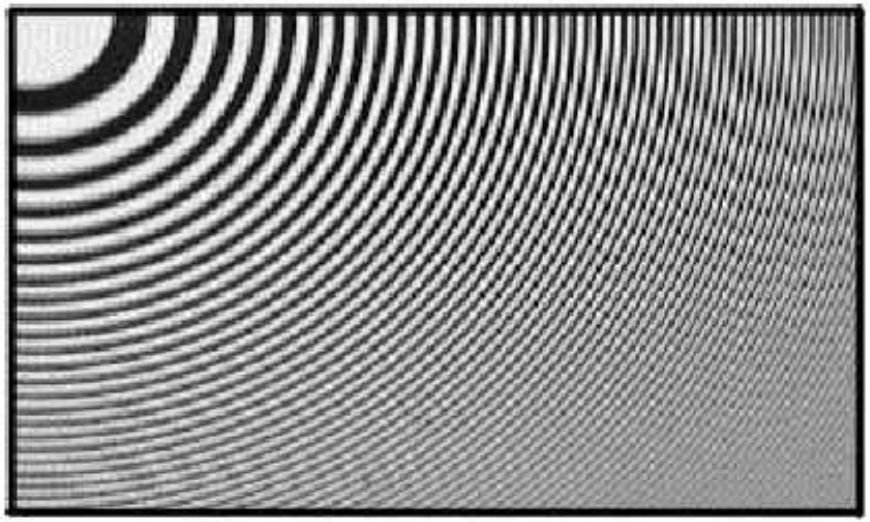

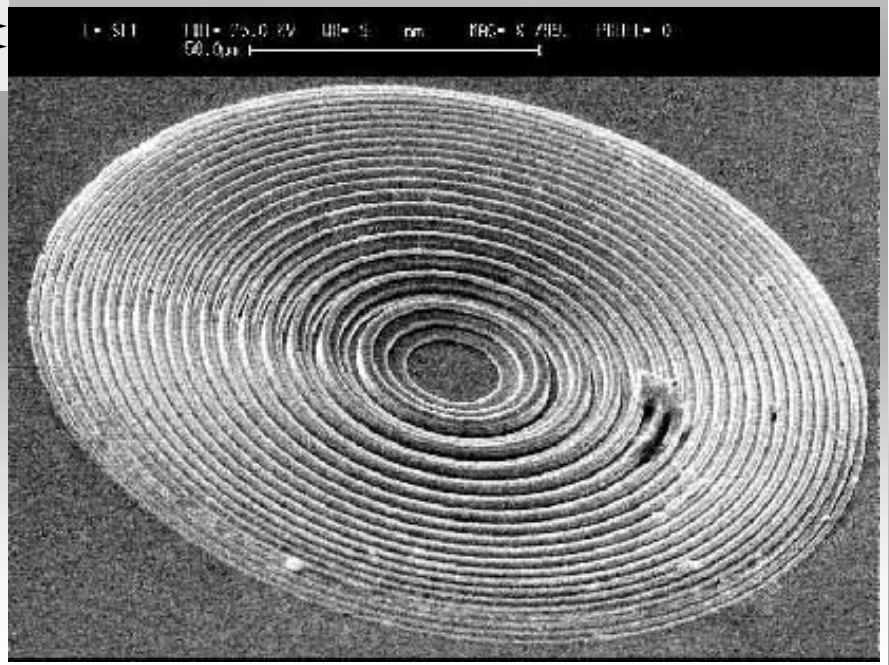

Spatial resolution

ultimate limit
practical limit
experimental limit

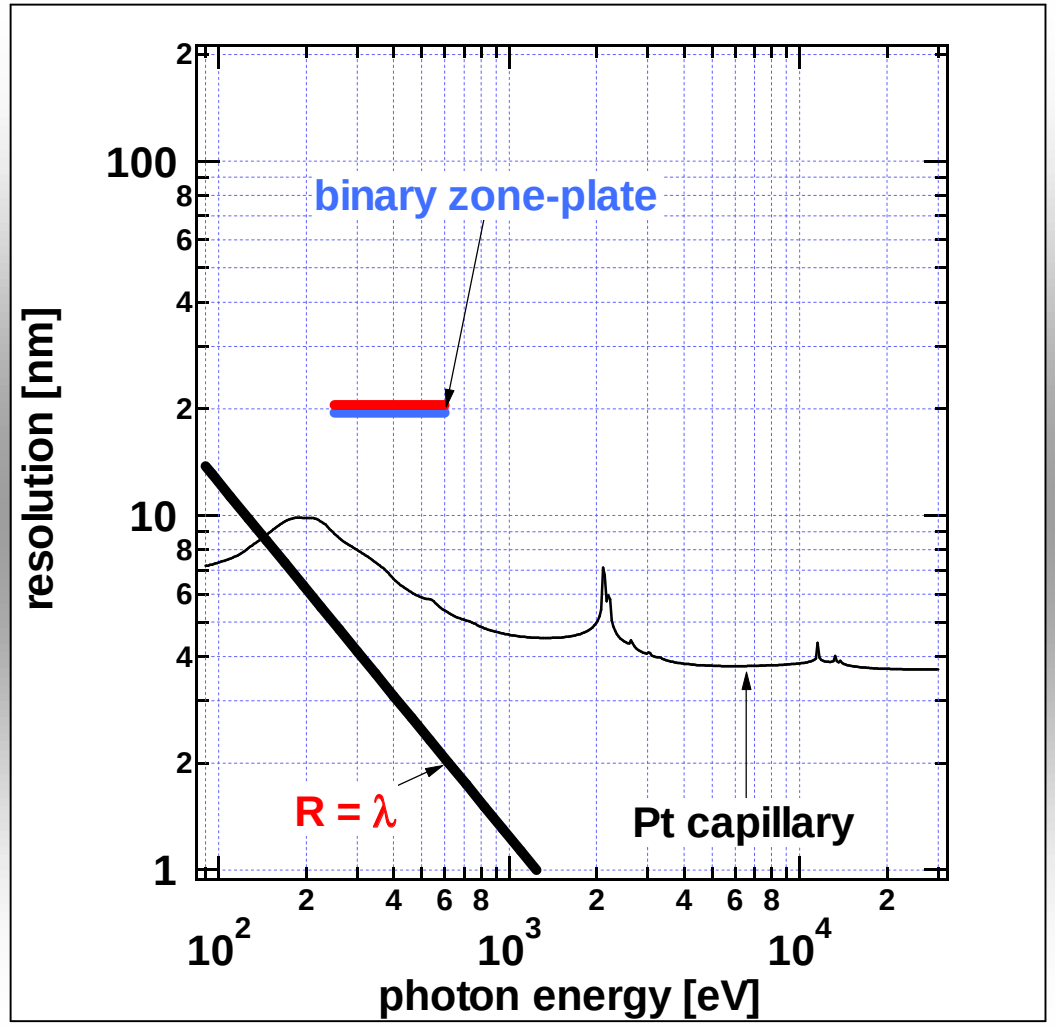

For binary zoneplates (opaque in soft x-rays)

r outermost period

R = r/2

$R_{prac} \approx 20$ nm

$R_{exp} \approx 20$ nm @ 2 nm (CXRO, Berkeley)

line width limit for lithographic processes

Spatial resolution

ultimate limit
practical limit
experimental limit

Rings (thickness t) become transparent for x-rays.
Need phase zoneplates:

rings retard by π
$t = \lambda/(2\delta)$ and for circular ZP
$r_{min} = t/8$ $R_{prac} = r/2 = \lambda/(32\delta)$
$R_{exp} \approx 90$ nm for r=206 nm
$t \approx 4.4\ r$ @ λ=0.154 nm
(Yun et al, RSI 1999)

C. David et al, APL 2001

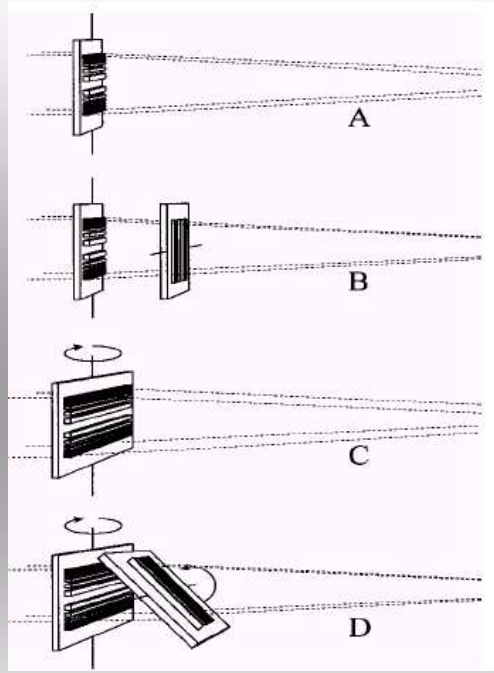

$r_{min} \approx t/50$ but $r_{min} > 40$ nm
$R_{prac} = \lambda/(200\delta) > 20$ nm

Spatial resolution

ultimate limit
practical limit
experimental limit

µXFA beamline and multilayer laboratory

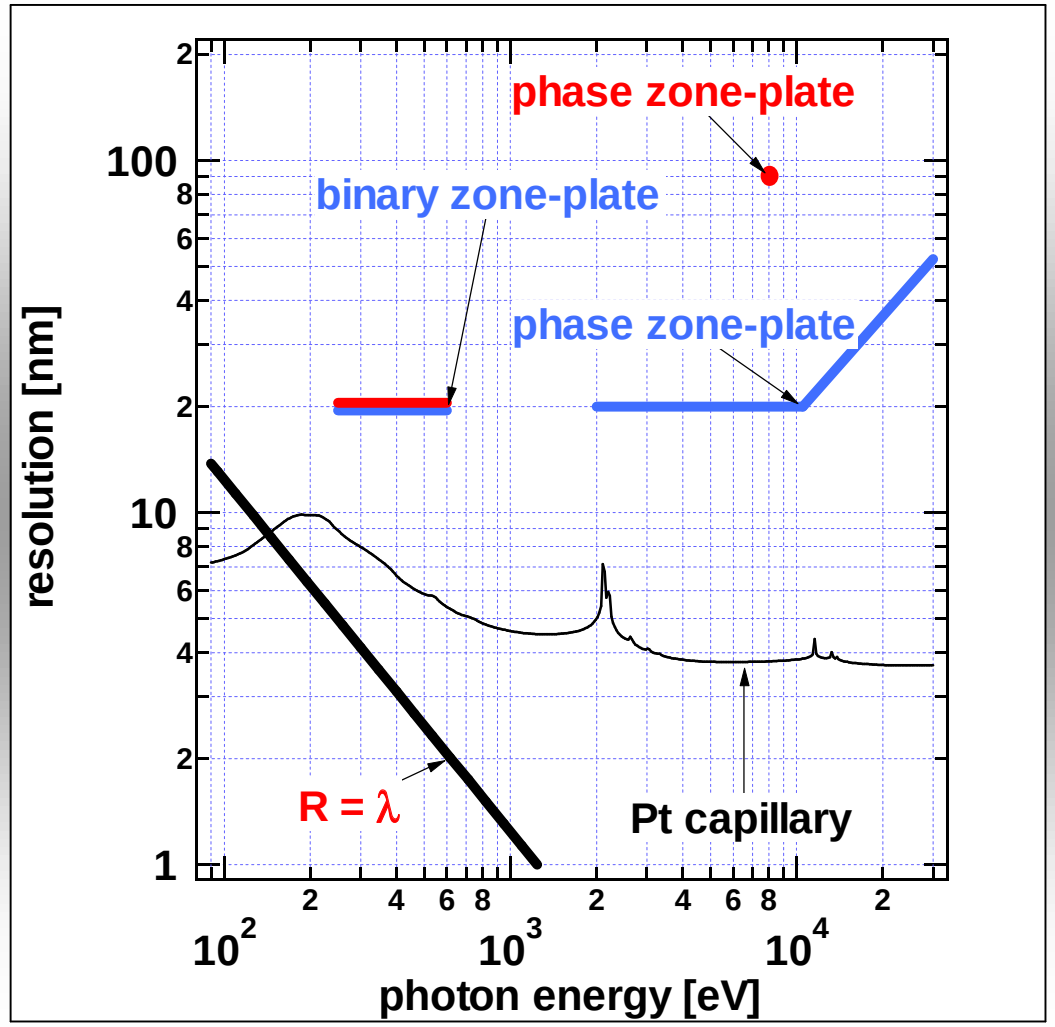

Phase zoneplates have better efficiency than binary zone-plates

out-of-phase zoneplates could produce smaller focii above 10 keV with reduced efficiency

Spatial resolution

ultimate limit
practical limit
experimental limit

Refraction

Compound refractive lenses (concave)
Snigirev et al, NATURE 1996

www.accel.de

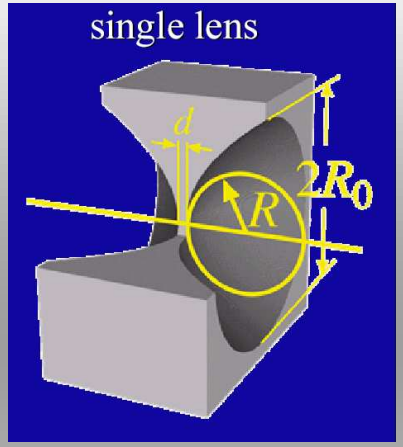

Lengeler
@SRI2003

Chromatic lenses

x-rays: $n = 1 - \delta - i\beta < 1$

need of concave and parabolic lenses

$f = Rad/\delta$ $\quad l = 1/(\rho*[\mu/\rho])$

lens transmission:

$T(y) = \exp(-y^2/2f\delta l)$

for d=0 Gaussian with

$\sigma = \sqrt{f\delta l}$

Spatial resolution

ultimate limit
practical limit
experimental limit

µXFA beamline and multilayer laboratory

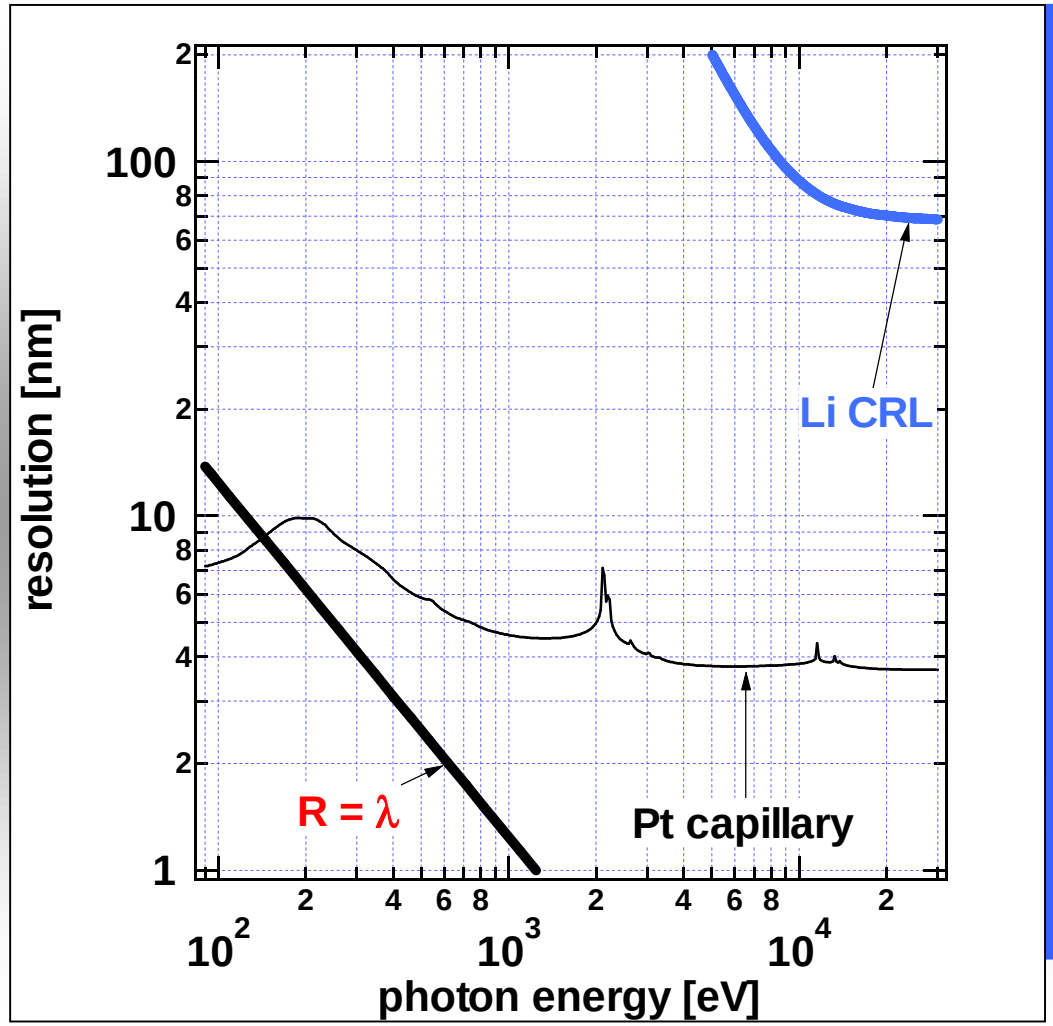

Best material lithium (more convenient beryllium, aluminum)

taken for (2 NA): fwhm opening =2.35 σ and f=200 mm

2 NA = 2.35 sqrt(δ l/f)
R_{prac}=sqrt(f/l)λ/sqrt(5.5 δ)

problem is source size S

Spatial resolution

ultimate limit
practical limit
experimental limit

Diffraction limited spot size is obtained with spatially coherent incident radiation

A = lens aperture **Q = source distance**

$$S\,(A/Q) = \lambda$$

$$\Longrightarrow$$

$$Q = SA/\lambda$$

e.g. S=30 µm, A=1 mm, λ =0.154 nm: Q=200 m!!

Couldn't it be better to compress the beam?

Spatial resolution

ultimate limit
practical limit
experimental limit

µXFA beamline and multilayer laboratory

X-ray waveguides

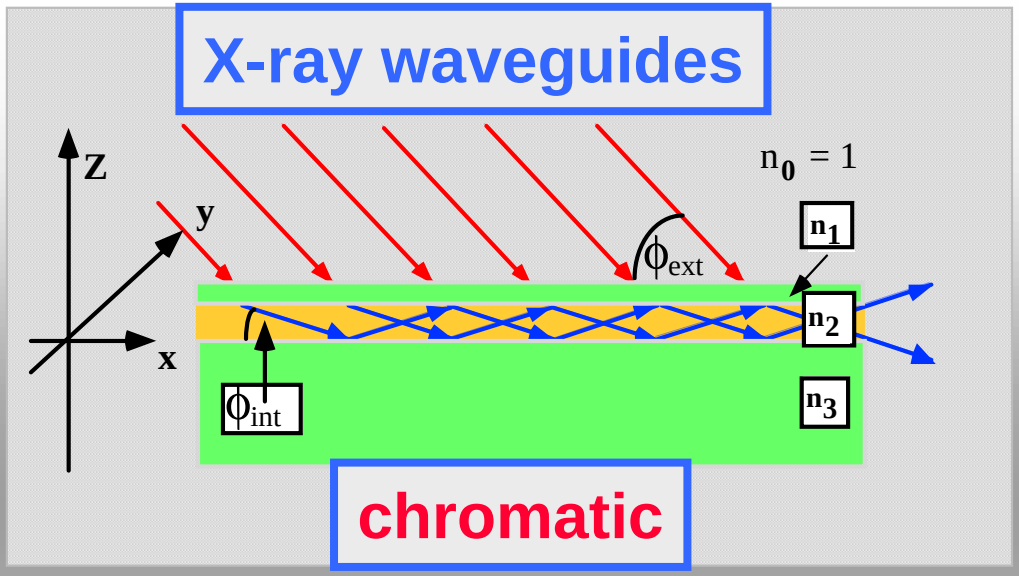

chromatic

Fwhm beam size at exit is D/2.
Beam to be reflected internally

$$\phi_{int} > \Phi_{crit}$$

is standing wave with

$$D = \lambda / 2 \sin \phi_{int}$$

Snell's law:

$$\phi_{ext} = \mathrm{sqrt}(\phi_{int}^2 + \phi_{crit}^2)$$

for $\delta_2 << \delta_3$:

$$D_{min} = \lambda/(2\ \mathrm{sqrt}(2\delta_3))$$

$$R_{ult} = \lambda/(4\ \mathrm{sqrt}(2\delta)) = R_{prac}$$

same for capillaries and tapered waveguides (Bergemann, PRL 2003)

equation is identical to single bounce capillary

Spatial resolution

ultimate limit
practical limit
experimental limit

µXFA beamline and multilayer laboratory

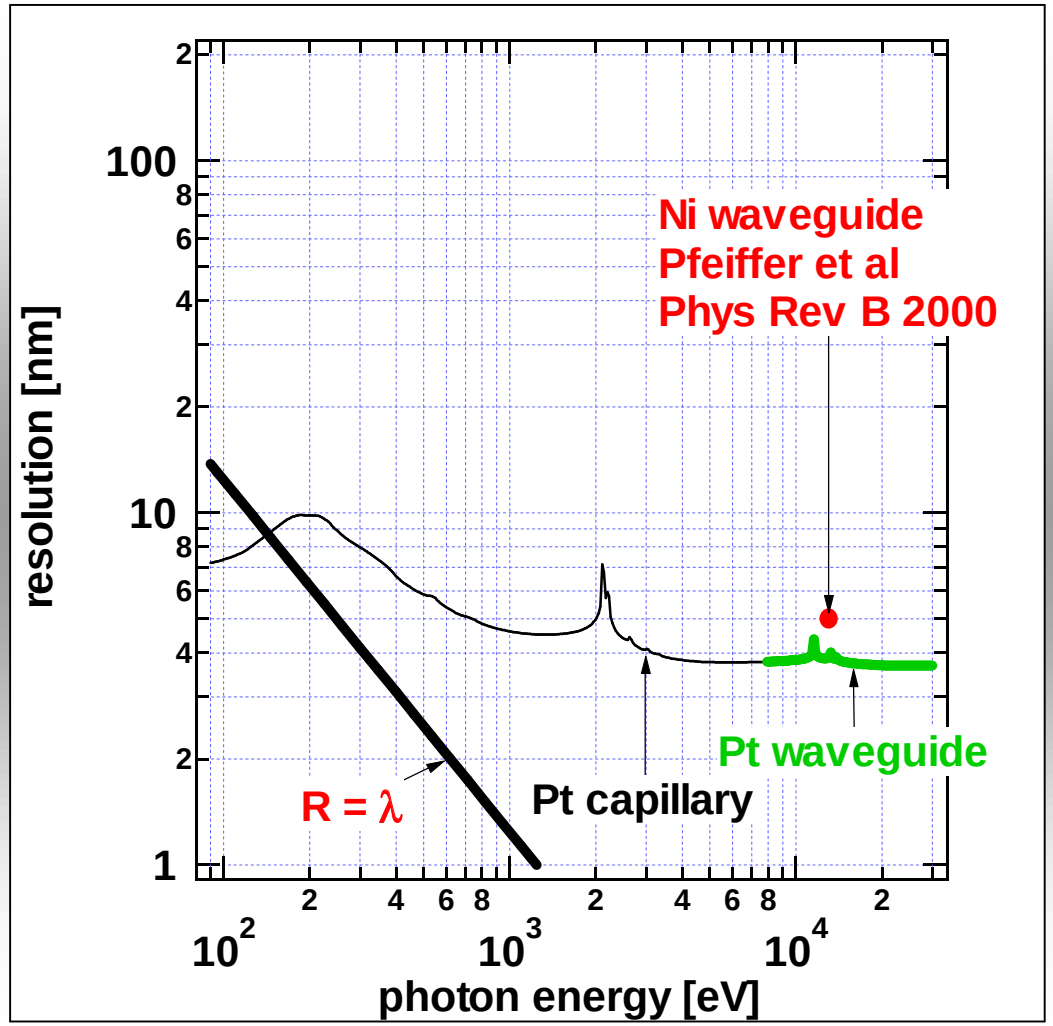

Waveguides rather inefficient with D=10 nm. However, D=70 nm and thus R=35 nm can be provided "easily" with high efficiency (Jark et al, APL 2001)

2-dimensional version was successfully produced (Pfeiffer et al, Science 2002)
R: 35 nm x 65 nm

Spatial resolution

ultimate limit
practical limit
experimental limit

In scanning configurations, may be better in imaging

• ellipsoids, toroids	R > 5000 nm
• mono-capillaries	R ≈ 5000 nm
• Kirkpatrick-Baez mirror pair (elliptical)	R = 83 nm
• Fresnel zone-plates	R = 20 … 50 nm
• compound refractive lenses CRL	R ≈ 200 nm
• x-ray waveguides	R ≈ 35 nm

What is the spot size?

µXFA beamline and multilayer laboratory

Classical knife-edge test

CRL: C.G. Schroer et al, APL 82, 1485 (2003)

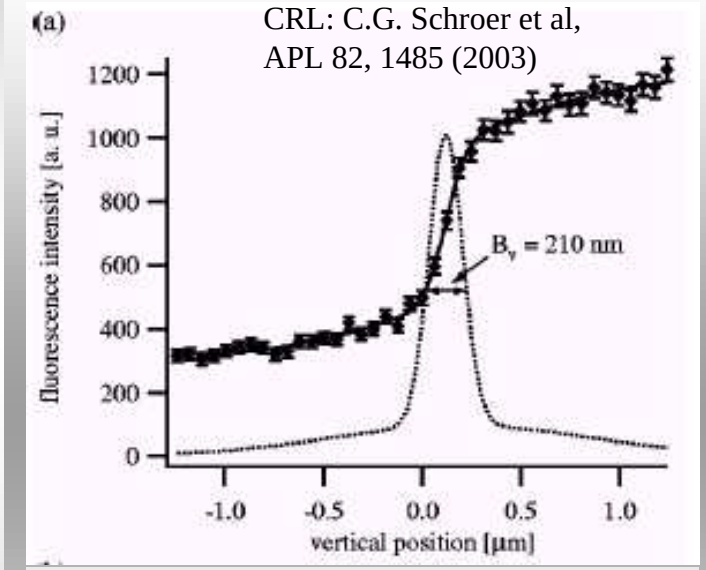

Fit to integrated data

Fluorescence from test pattern A.C. Thomson et al, Proc. SPIE 4145, 16 (2000)

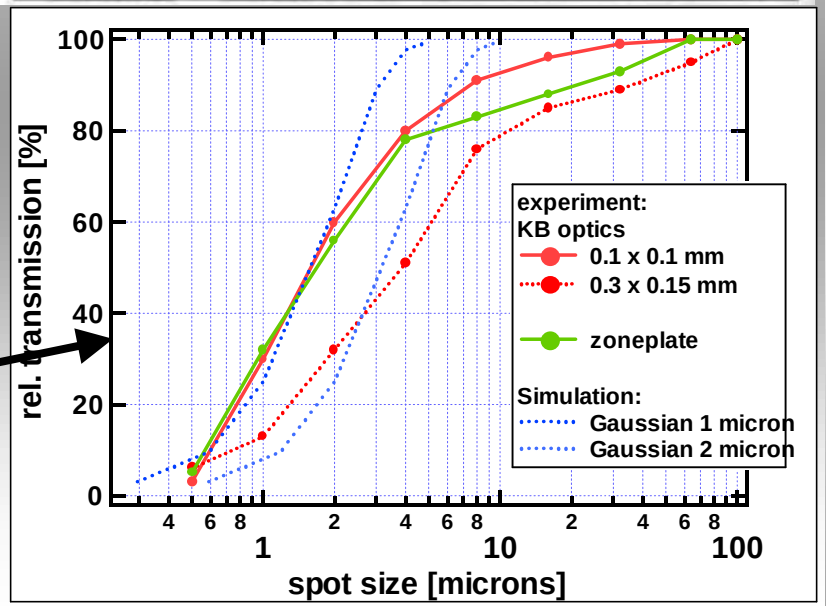

claimed knife-edge fwhm resolution:
KB mirrors: 1 µm x 1 µm
zone-plate: 0.15 µm x 0.2 µm

X-ray Zoom lens: Do-It-Yourself!

µXFA beamline and multilayer laboratory

1

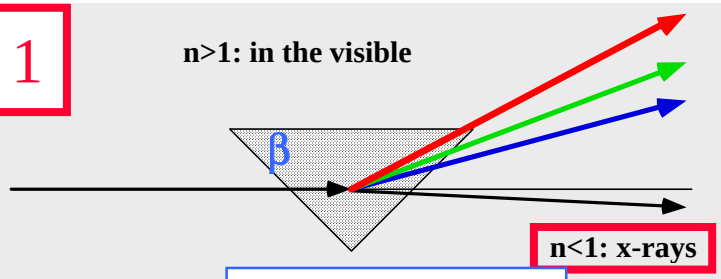

$\Delta\theta = 2(1-n)/\tan\beta$

2

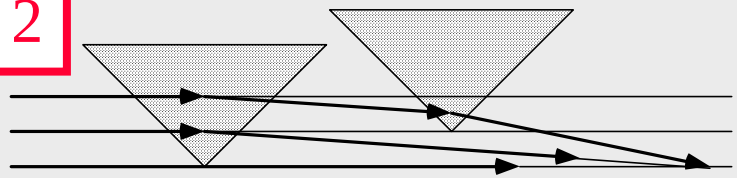

many

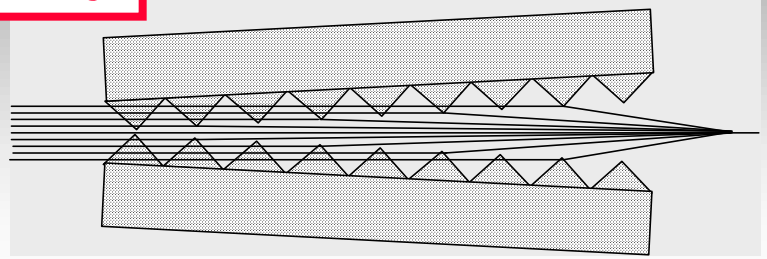

B. Cederström, R. N. Cahn, M. Danielsson, M. Lundqvist, D. R. Nygren:
Focusing x-rays with old LP's
Nature 404, 951 (2000)

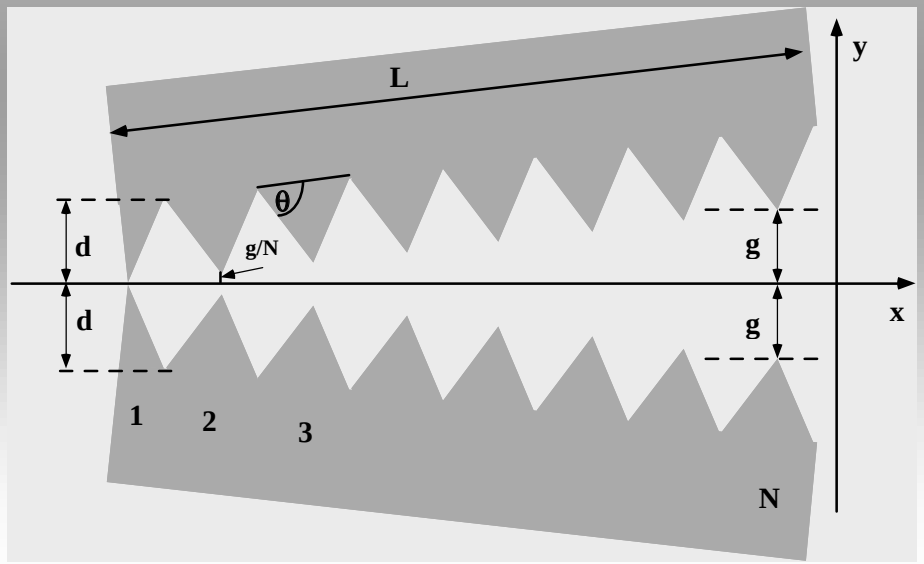

Get it almost for free

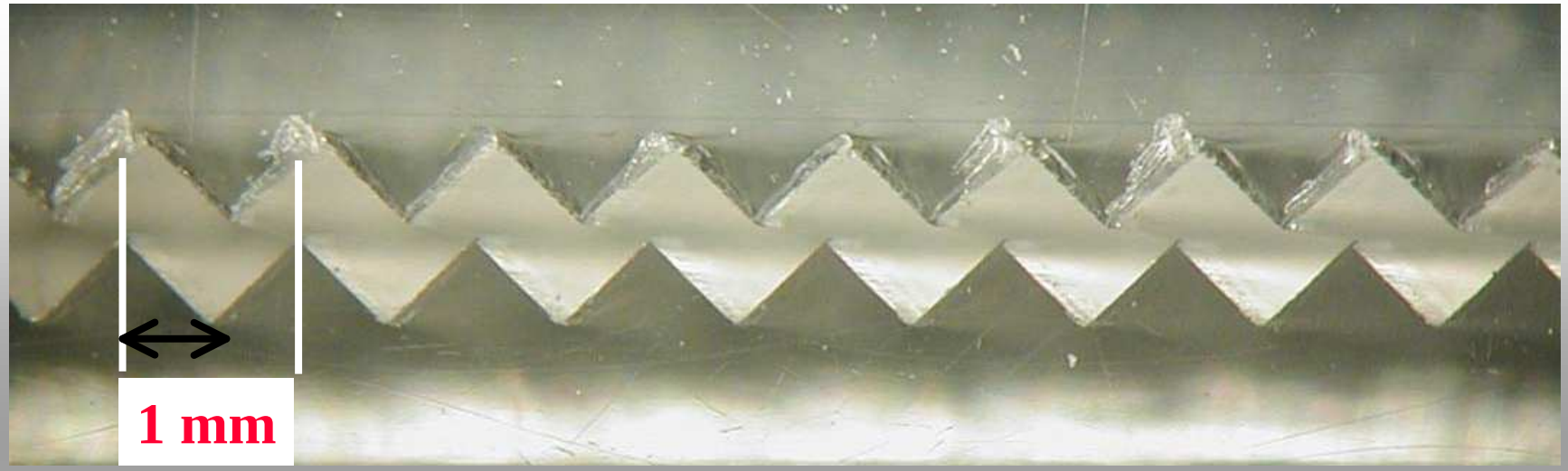

Sawtooth comb milled into PLEXIGLASS in ELETTRA workshop [Marco De Gregorio, Gilio Sandrin]

For geometrical optics it is a lens with parabolic transmission function, i.e. an approximation of CRL

Test it at home

µXFA beamline and multilayer laboratory

x-ray tube
(35 kV white)
0.04 mm x 4 mm

alligator lens in PMMA
50 teeth over 50 mm
vert. acc. 0.15 mm for 12 keV
opening 0.2 mm (2 µm pitch)

Si(Li) detector
behind 0.01 mm slit
expected beam size:
without lens: 0.3 mm
with lens: 0.04 mm

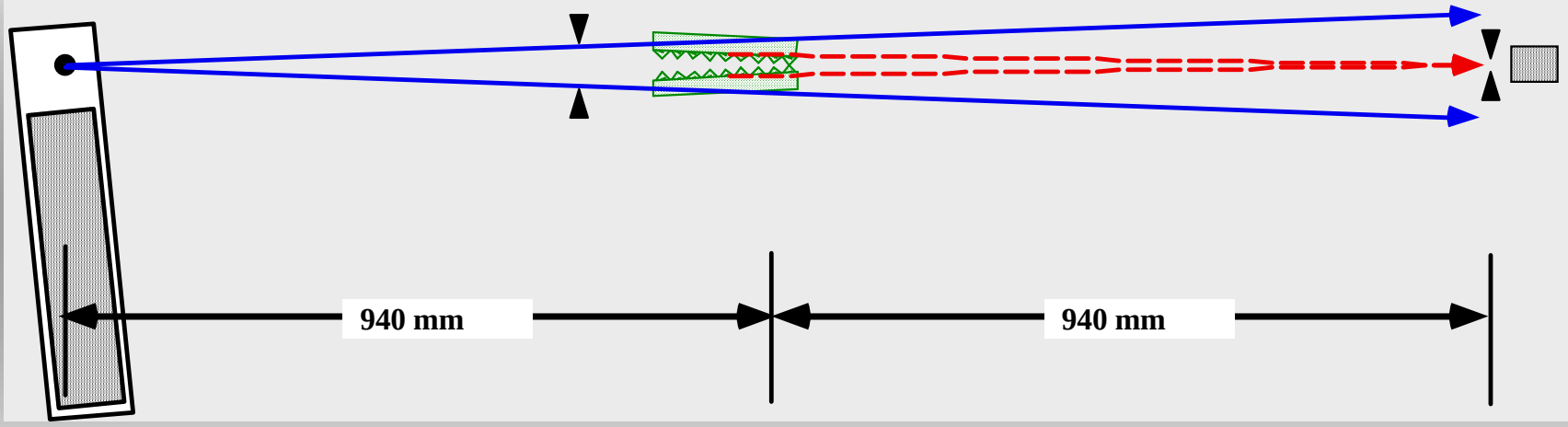

With an average transmission of 0.85 in the effective aperture an intensity gain of **g = 0.85 * 0.3/0.04 = 6.3** is expected

Results

You get gain!

And you have an easily tunable large bandpass x-ray monochromator!

Interesting also as beam collimator

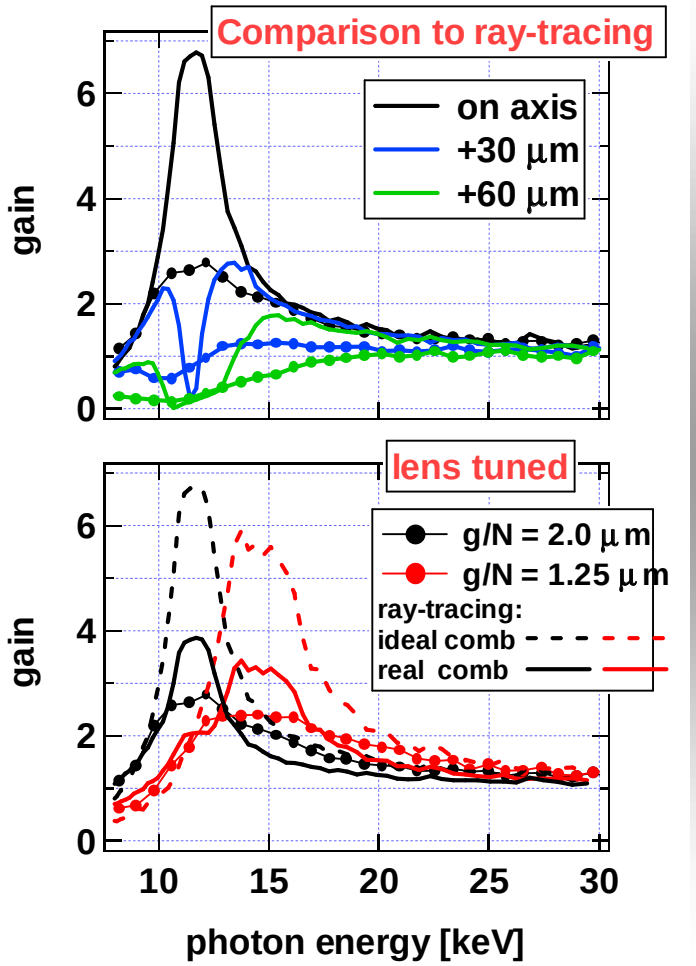

A tiny plastic x-ray lens

µXFA beamline and multilayer laboratory

How to reduce absorption in CRL's?

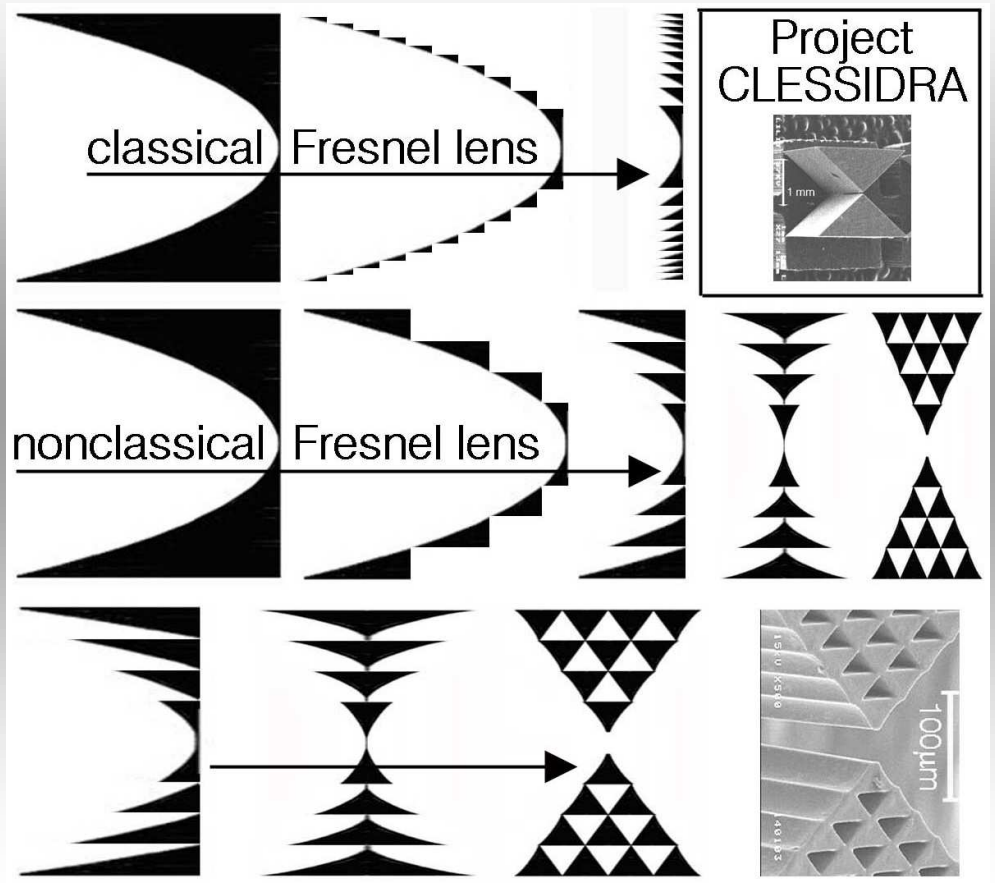

Beryllium Lenses

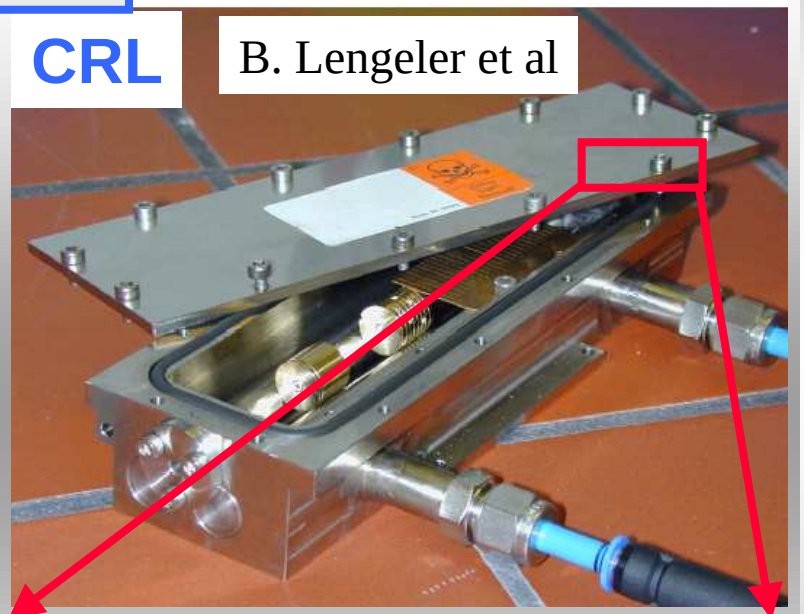

Clessidra

A tiny plastic x-ray lens!

µXFA beamline and multilayer laboratory

Jark et al, JSR 2004

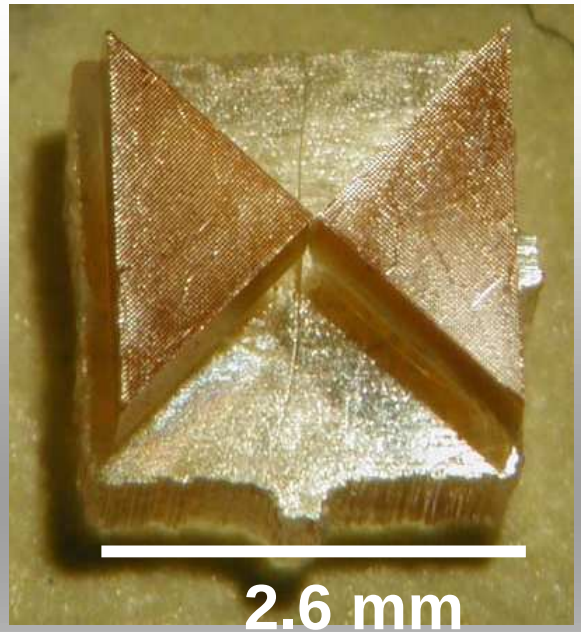

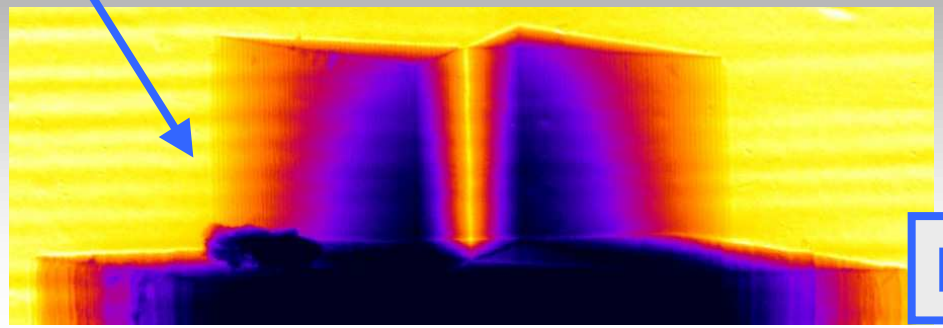

Effective aperture similar to CRL's. f=1 m ... 2 m for λ=0.154 nm

Exp. focus 2.8 µm! At ELETTRA 15x intensity gain in one dimension in 30 µm spot!

High resolution radiograph

A tiny plastic x-ray lens!

µXFA beamline and multilayer laboratory

Two-dimensional focus behind crossed lenses

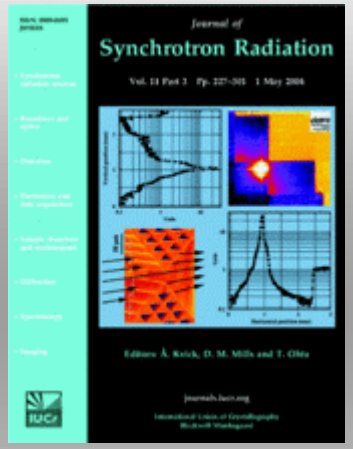

Jark et al, JSR 2004

CCD image:

lens shadow

focus, gain 25x

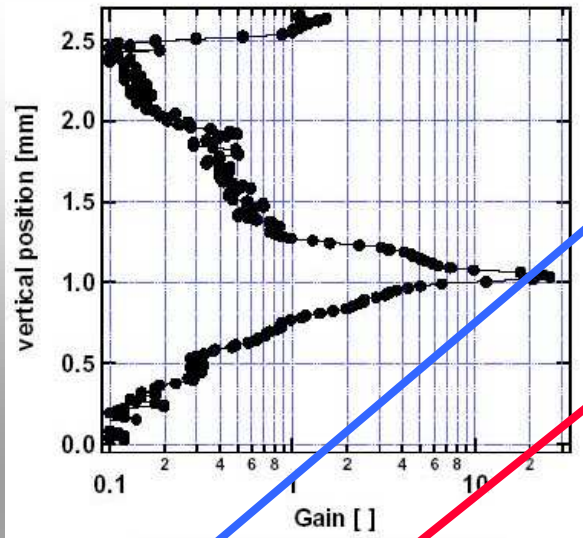

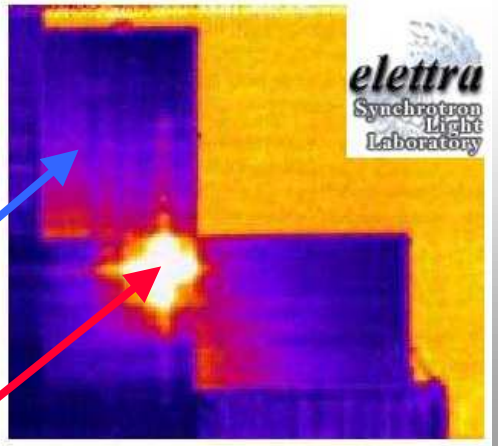

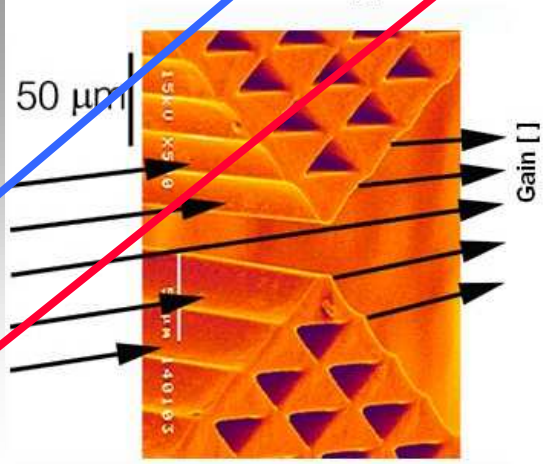

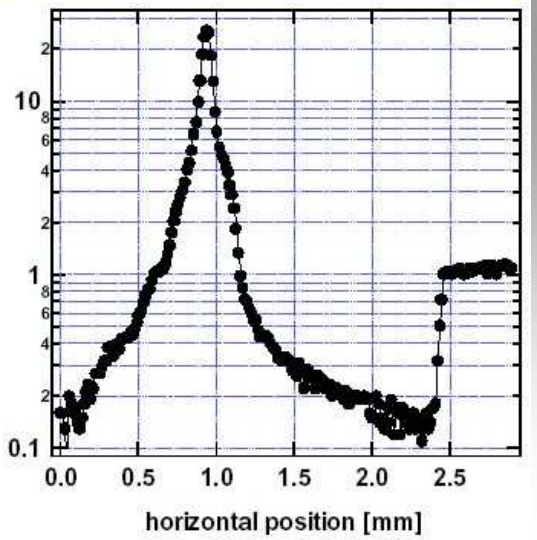

JOURNAL OF THE OPTICAL SOCIETY OF AMERICA VOLUME 38, NUMBER 9 SEPTEMBER, 1948

1948

Formation of Optical Images by X-Rays

PAUL KIRKPATRICK AND A. V. BAEZ
Stanford University, Stanford, California
(Received March 12, 1948)

Several conceivable methods for the formation of optical images by x-rays are considered, and a method employing concave mirrors is adopted as the most promising. A concave spherical mirror receiving radiation at grazing incidence (a necessary arrangement with x-rays) images a point into a line in accordance with a focal length $f = Ri/2$ where R is the radius of curvature and i the grazing angle. The image is subject to an aberration such that a ray reflected at the periphery of the mirror misses the focal point of central rays by a distance given approximately by $S = 1.5Mr^3/R$, where M is the magnification of the image and r is the radius of the mirror face. The theoretically possible resolving power is such as to resolve point objects separated by about 70Å, a limit which is independent of the wave-length used. Point images of points and therefore extended images of extended objects may be produced by causing the radiation to reflect from two concave mirrors in series. Sample results are presented.

INTRODUCTION

THE literature of x-rays contains many passages deploring the supposed impossibility of focusing x-rays with lenses or mirrors. Both the difficulty and the regret are easily appreciated. A satisfactory x-ray microscopy would open up fields of investigation closed to the optical microscope because of its restricted resolution, and to the electron microscope because of the limited penetrating power of electrons. X-ray spectrometers and diffraction instruments would probably have evolved along simpler or more advantageous lines had their designers possessed the means of optical control available to workers with light in other spectral regions.

X-RAY LENSES

Roentgen's[1] first experiments convinced him that x-rays could not be concentrated by lenses; thirty years later his successors understood why. X-ray refractive indices are less than unity by an amount δ which for common solids and x-rays of general practice has a value of the order of 10^{-5}. It may readily be shown that the focal length f of a single refracting surface of radius R is approximately R/δ. For several surfaces in series, arranged cooperatively, we have $1/f = \delta(1/R_1 + 1/R_2 + \text{etc.})$. To make a successful lens we require a large δ and slight absorption. Unfortunately ma-

[1] W. C. Roentgen, *Sitzungsberichte der Würzburger Physikalischen-Medicinischen Gesellschaft* (1895).

originally proposed for x-ray imaging

however,

today almost exclusively used for creation of small spots

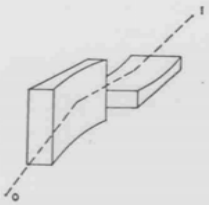

FIG. 11. Arrangement of concave mirrors to produce real images of extended objects with incidence at small grazing angles.

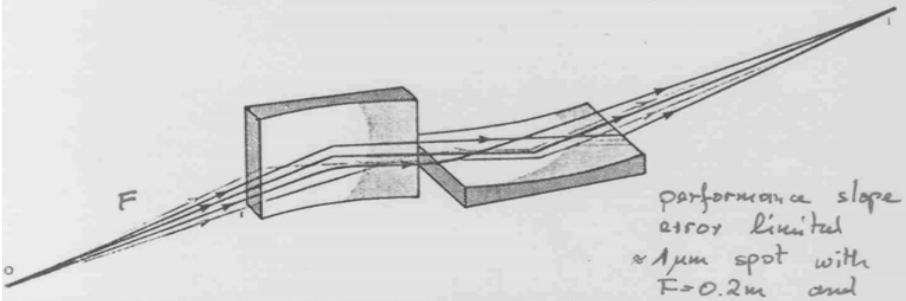

performance slope error limited
≈1μm spot with F=0.2m and 0.25" rms

Microscope principle that corrects the astigmatism associated with glancing-incidence spherical mirrors. Kirkpatrick–Baez microscopes based on this method of crossed mirrors are used to make x-ray photographs of the implosions of laser-fusion capsules.

Figure 4

Collection of historical documents

Schwarzschild objective

suggested for use with multilayer coatings in the soft x-ray range at DESY, Hamburg, Germany:

P.-P. Haelbich, W. Staehr and C. Kunz
Ann. N. Y. Acad. Sci., New York, 342, 148 (1980)

classical application: long distance objective for full field microscopy

here it is used in the reversed (demagnifying) orientation

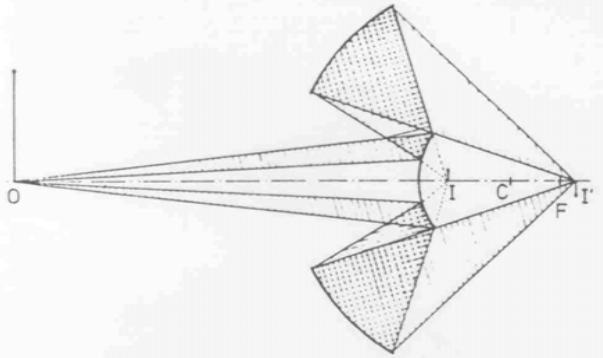

Fig. 11. Cross section of a Schwarzschild objective with two spherical mirrors (from Haelbich et al. (1980)). Example for the actual parameters for a 10× objective with an aperture angle $\sin\frac{1}{2}\theta_a = 0.125$: diameter and radius of curvature for the big mirror, 4.4 and 13.409 cm, for the small mirror, 1 and 5.205 cm, mirror spacing 8.387 cm. (Example by R. Tibbetts, IBM.)

spot diameter < 0.1 μm achieved
very little tuning capabilities
performance limited by scattering producing significant tails

US005684852A

United States Patent [19]
Tomie

[11] Patent Number: 5,684,852
[45] Date of Patent: Nov. 4, 1997

[54] X-RAY LENS

[75] Inventor: Toshihisa Tomie, Tsukuba, Japan

[73] Assignee: Agency of Industrial Science & Technology, Ministry of International Trade & Industry, Tokyo, Japan

[21] Appl. No.: 736,680

[22] Filed: Oct. 25, 1996

Related U.S. Application Data

[62] Division of Ser. No. 389,501, Feb. 16, 1995, Pat. No. 5,594,773.

[30] Foreign Application Priority Data

Feb. 18, 1994 [JP] Japan 6-45248

[51] Int. Cl.[6] G21K 1/06

[52] U.S. Cl. 378/145; 378/84; 250/505.1; 359/665; 359/811

[58] Field of Search 359/565, 569, 359/709, 730, 741, 742, 743-747, 811; 378/145, 84, 140; 250/505.1

[56] References Cited

U.S. PATENT DOCUMENTS

3,734,804 4/1973 Leaheat et al. 359/710

Primary Examiner—Duc Wong
Attorney, Agent, or Firm—Oblon, Spivak, McClelland, Maier & Neustadt, P.C.

[57] ABSTRACT

An X-ray lens includes a plurality of hollow cylinders of prescribed radius bored in a lens material piece having a phase lag coefficient appropriate for the wavelength of the X-rays to be focused such that the axes of the hollow cylinders are parallel and perpendicularly intersect a straight array axis.

38 Claims, 9 Drawing Sheets

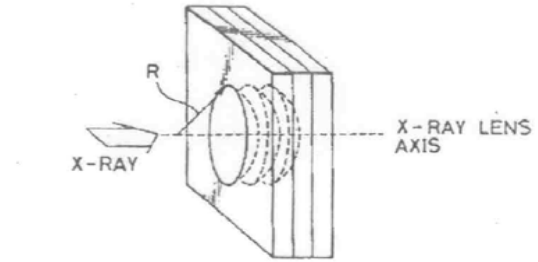

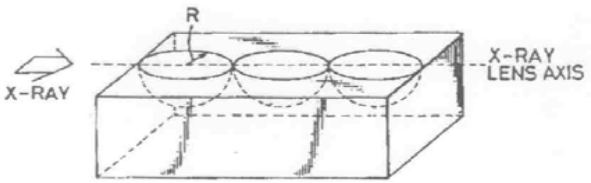

FIG. 3

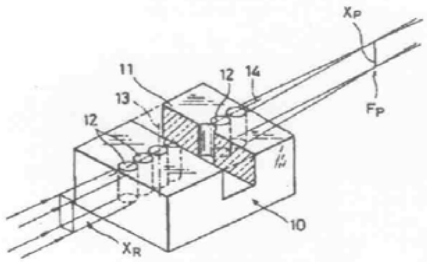

A compound refractive lens for focusing high-energy X-rays

A. Snigirev*, V. Kohn†, I. Snigireva* & B. Lengeler*‡

* European Synchrotron Radiation Facility, BP220, F-38043 Grenoble Cedex, France
† Kurchatov, I. V., Institute of Atomic Energy, 123182 Moscow, Russia

The development of techniques for focusing X-rays has occupied physicists for more than a century. Refractive lenses, which are used extensively in visible-light optics, are generally considered inappropriate for focusing X-rays, because refraction effects are extremely small and absorption is strong. This has lead to the development of alternative approaches[1,2] based on bent crystals and X-ray mirrors, Fresnel and Bragg–Fresnel zone plates, and capillary optics (Kumakhov lenses). Here we describe a simple procedure for fabricating refractive lenses that are effective for focusing of X-rays in the energy range 5–40 keV. The problems associated with absorption are minimized by fabricating the lenses from low-atomic-weight materials. Refraction of X-rays by one such lens is still extremely small, but a compound lens (consisting of tens or hundreds of individual lenses arranged in a linear array) can readily focus X-rays in one or two dimensions. We have fabricated a compound lens by drilling 30 closely spaced holes (each having a radius of 0.3 mm) in an aluminium block, and we demonstrate its effectiveness by focusing a 14-keV X-ray beam to a spot size of 8 μm.

The index of refraction for X-rays in matter can be written as $n = 1 - \delta + i\beta$, where β is the absorption index and δ is the refractive index decrement. Refraction being very small (δ is typically between 10^{-5} and 10^{-7}), all attempts to date to build refractive lenses for X-rays have been unsuccessful. Recently, the discussion about refractive lenses has been revived. Suehiro, Miyaji and Hayashi[3] have proposed a refractive lens of high-atomic-number (high-Z) material for focusing X-rays. Michette[4]

‡ Present address: Physikalisches Institut, RWTH Aachen, 52056 Aachen, Germany.

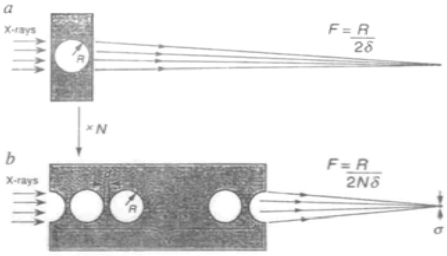

FIG. 1 Schematic diagram showing the principles of X-ray focusing by a compound refractive lens (CRL). As $(1 - \delta)$ is smaller than 1 (where δ is the decrement of the refractive index), a collecting lens for X-rays must have a concave shape. *a*, A simple concave lens fabricated as a cylindrical hole in the material. *b*, A CRL consisting of a number (N) of cylindrical holes placed close together in a row along the optical axis, focuses the X-rays at a distance that is N times shorter compared to a single lens. R is the radius of the holes, d is the spacing between the holes, λ is the X-ray wavelength, and F is the focal distance for a parallel input beam.

latest improvements

Fig. 3. Schematic view of the parabolically shaped single and compound refractive lenses: R, radius of curvature; A, aperture of the lens; p, length of the single lens or the distance between the centers of the two neighboring holes for a compound lens. (a) Single parabolic refractive lens, (b) compound refractive lens with parabolically shaped holes, (c) compound refractive lens with parabolically shaped half-holes.

Table 1. Calculated CRL Parameters for Boron and Aluminum*

Lens Material, Hole Radius, R Focal Distance, F	Energy, E (keV)	Number of Holes, N	Effective Aperture, A (μm)	Resolution σ (μm)	Real Gain, g	Length, L (mm)
B R = 500 μm F = 1 m	5	13	251	1	190	13
	10	55	211	0.6	186	55
	20	222	177	0.4	168	224
	30	501	160	0.3	166	506
	40	892	149	0.2	176	901
Al R = 500 μm F = 1 m	10	45	116	1	6	45
	20	184	163	0.4	36	186
	30	417	160	0.3	60	421
	40	743	149	0.2	80	750

*Calculations were made in the following conditions: source size, 50 μm; source–lens distance, 50 m; lens focal distance, F = 1 m; spacing between holes, d = 10 μm. G is the ideal gain in the intensity at the focus for a point source. The real gain g takes into account the finite source size and the attenuation of the x rays owing to absorption in the material between the holes.

Nanometer Spatial Resolution Achieved in Hard X-ray Imaging and Laue Diffraction Experiments

Donald H. Bilderback,* Stephen A. Hoffman, Daniel J. Thiel

Tapered glass capillaries have successfully condensed hard x-ray beams to ultrasmall dimensions providing unprecedented spatial resolution for the characterization of materials. A spatial resolution of 50 nanometers was obtained while imaging a lithographically prepared gold pattern with x-rays in the energy range of 5 to 8 kiloelectron volts. This is the highest resolution scanning x-ray image made to date with hard x-rays. With a beam 360 nanometers in diameter, Laue diffraction was observed from the smallest sample volume ever probed by x-ray diffraction, 5×10^{-3} cubic micrometers.

spot ϕ 0.05 μm achieved

routinely used with good gain 1 μm

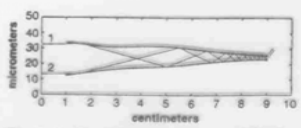

Fig. 1. Profile of the inner diameter (ID) of a capillary measured with an optical microscope. The entering ID is 22 μm and the exit ID is 3 μm. The calculated trajectories of two rays from a parallel x-ray beam are shown. Ray 1 undergoes 12 successive bounces with a net throughput of 57%, as calculated by a two-dimensional ray-tracing program that includes the x-ray reflectance for each bounce. Ray 2 undergoes 11 reflections with a net throughput of 61%. The average reflectivity per bounce exceeds 95%, and the total deflection angles are 2.3 and 2.2 mrad, respectively.

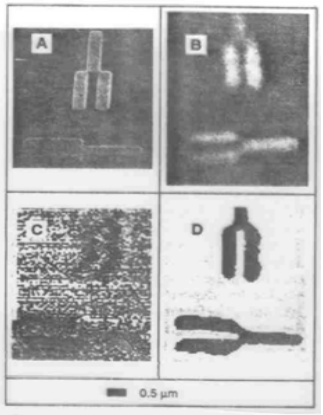

Fig. 2. Various images of a lithographically prepared test sample consisting of a 100-nm-thick gold pattern deposited on a 200-nm-thick Si_3N_4 substrate. The line widths of the features are 300 nm. (**A**) Scanning electron micrograph. (**B**) Optical image obtained with a visible-light microscope with a numerical aperture of 0.9. The image is blurred because the structure has features below the resolving power of the microscope. (**C**) Unprocessed x-ray absorption image. The image was formed from a two-dimensional scan consisting of 50 nm by 50 nm pixels. (**D**) X-ray image after processing. The data in each row were horizontally shifted to compensate for the effects of spatial drift (thermal, air currents, electronic, and so on). A median processor was then applied, which averages all pixel intensities located in a circle of radius 2 pixels.

SCIENCE • VOL. 263 • 14 JANUARY 1994

J. Synchrotron Rad. (1994). **1**, 37–42

X-ray Applications with Glass-Capillary Optics

D. H. Bilderback,[a,b] D. J. Thiel,[a,c] R. Pahl[a] and K. E. Brister[a]

[a]Cornell High Energy Synchrotron Source (CHESS), [b]School of Applied and Engineering Physics, and [c]Department of Biochemistry, Cell and Molecular Biology, Cornell University, Ithaca, NY 14853, USA

(Received 23 May 1994; accepted 23 June 1994)

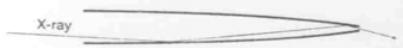

Figure 1
An X-ray beam can efficiently be transmitted through a capillary concentrator if reflection from the smooth walls takes place at angles less than the critical angle of reflection. For hard X-rays and typical borosilicate glasses, the critical angle for 10 keV X-rays is about 3 mrad or 0.2°.

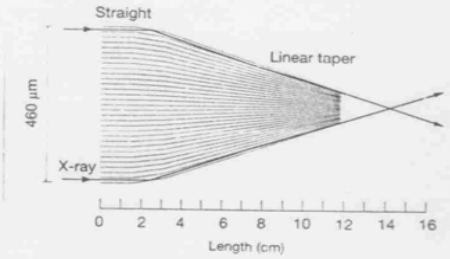

Figure 2
Schematic diagram of X-rays passing through a perfect poly-capillary concentrator. A device has been used to condense 6 keV X-rays to a diameter of 68 μm while enhancing the intensity (flux/area) by a factor of 5 (Hoffman *et al.*, 1994*b*). Before pulling, the concentrator consisted of 330 parallel tubes of 18 μm inner diameter and 2 μm wall thickness (Gibson, 1994).

Journal of Synchrotron Radiation
ISSN 0909-0495 © 1994

brief communications

Focusing hard X-rays with old LPs

A vinyl long-playing record can be used to form a cheap, aberration-free refractive lens.

Björn Cederström*, Robert N. Cahn†, Mats Danielsson*, Mats Lundqvist*, David R. Nygren†

**Department of Physics, Royal Institute of Technology, SE-104 05 Stockholm, Sweden e-mail: ceder@particle.kth.se*

†Physics Division, Lawrence Berkeley National Laboratory, Berkeley, California 94720, USA

NATURE | VOL 404 | 27 APRIL 2000 | www.nature.com

In the small-angle approximation, a ray traverses the saw-tooth refractive lens in a straight line parallel to the optical axis. A ray separated by y from the optical axis traverses a thickness of material given by $x(y) = y^2 N/(y_s \tan\theta)$

This is a parabola, with radius of curvature $R = y_s \tan\theta/2N$

The total length of the lens is $L = 2Ny_s/\tan\theta$, and so $R = (y_s/2N)(2y_sN/L) = y_sy/L$.

Thus we can treat the saw-tooth refractive lens as a single parabolic lens with a focal length of $f = R/\delta$, where δ is the decrement of the real part of the index of refraction from unity (typically 10^{-6} for hard X-rays). The focusing properties are independent of the fixed free parameter θ.

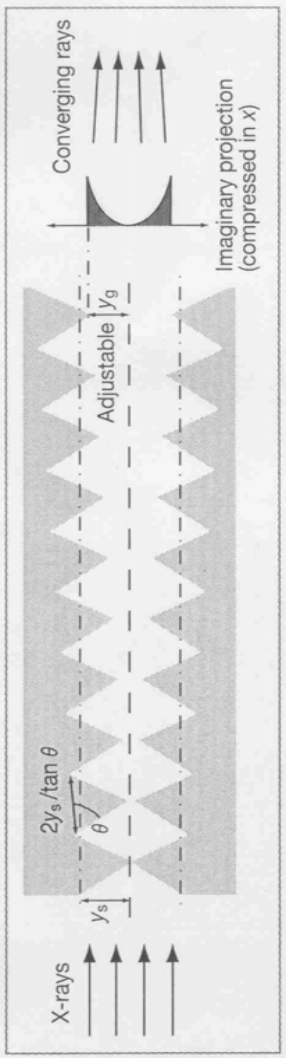

Figure 1 The saw-tooth refractive lens for hard X-rays. Only ten of 300 teeth are shown. The lens bears a striking resemblance to phonograph records, the groove pitch of which is about 180 μm. Measurements of the profile indicate that the depth of the groove is insufficient (about 25μm) and that there is a large amount of material between the grooves, however, resulting in unnecessary X-ray attenuation. We therefore had a dedicated master cut with a groove depth of 90 μm, from which a vinyl record was pressed. Two 60-mm long sections were cut out to form the lens. With 180 μm separation at the end, the focal length is 218 mm for 23-keV X-rays.

S. Di Fonzo et al, Nature 403, 638 (2000)

21. Bakhshi, A. K. Investigation of electronic conduction in proteins and DNA. Prog. Biophys. Mol. Biol. **60**, 187–253 (1994).
22. Ladik, J. Energy bands in DNA. *Int. J. Quantum Chem.* **4**, 307–317 (1971).

Acknowledgements

We thank L. Gurevich for assistance in the fabrication and measurements; E. W. J. M. van der Drift, A. van der Enden, L. E. M. de Groot, S. G. Lemay, A. K. Langen-Suurling, R. N. Schouten, Z. Yao, T. Zijlstra, M. R. Zuiddam, M. P. de Haas, J. M. Warman, A. Storm, N. Kemding and J. Jortner for assistance and discussions; and E. Kramer and E. Yildirim for the DNA characterization measurements. This work was supported by the Dutch Foundation for Fundamental Research on Matter (FOM).

Correspondence and requests for materials should be addressed to C.D. (e-mail: dekker@qt.tn.tudelft.nl).

Non-destructive determination of local strain with 100-nanometre spatial resolution

S. Di Fonzo*, W. Jark*, S. Lagomarsino†, C. Giannini‡, L. De Caro‡, A. Cedola†§ & M. Müller§

* *SINCROTRONE TRIESTE, SS 14 km 163.5 in Area Science Park, I-34012 Basovizza - Trieste, Italy*
† *Istituto Elettronica Stato Solido (IESS) - CNR, V. Cineto Romano 42, I-00156 Roma, Italy*
‡ *Centro Nazionale Ricerca e Sviluppo Materiali (PASTIS-CNRSM), Strada Statale 7 Appia km 712, I-72100 Brindisi, Italy*
§ *ESRF, BP 220, F-38043 Grenoble Cedex, France*

Structure sizes of ~180 nm are now standard in microelectronics, and state-of-the-art fabrication techniques can reduce these to just a few tens of nanometres (ref. 1). But at these length scales, the strain induced at interfaces can locally distort the crystal lattice, which may in turn affect device performance in an unpredictable way. A means of non-destructively characterizing such strain fields with high spatial resolution and sensitivity is therefore highly desirable. One approach is to use Raman spectroscopy[2], but this is limited by the intrinsic ~0.5-μm resolution limit of visible light probes. Techniques based on electron-beam diffraction can achieve the desired nanometre-scale resolution. But either they require complex sample preparation procedures[3] (which may alter the original strain field) or they are sensitive to distortional (but not dilational) strain within only the top few tens of nanometres of the sample surface[4,5]. X-rays, on the other hand, have a much greater penetration depth, but have not hitherto achieved strain analysis with sub-micrometre resolution[6]. Here we describe a magnifying diffraction imaging procedure for X-rays which achieves a spatial resolution of 100 nm in one dimension and a sensitivity of 10^{-4} for relative lattice variations. We demonstrate the suitability of this procedure for strain analysis by measuring the strain depth profiles beneath oxidized lines on silicon crystals.

The crucial element of our set-up is a waveguide[7,8] (WG in Fig. 1), which constitutes an unusual optical element for medium- and high-energy X-rays (10–30 keV). Unlike diffracting optical elements it does not focus a collimated incident beam, but instead confines it (through a resonance effect[9]) in one direction to a dimension of typically 100–150 nm, the distance between the parallel interfaces of the resonator[8]. Several resonator modes can be excited; these modes can leave at the end of the waveguide, with a high degree of spatial coherence in the plane perpendicular to the waveguide surface, which is here the vertical one. In this direction, the beam profile of the first resonance mode—at distances of more than 1 mm from the waveguide end—is well described by a gaussian beam[10,11]; this mode then seems to originate from a virtual line source inside the resonator. This has allowed us to register an in-line hologram with a spatial resolution of 140 nm in one direction[12].

The idea behind the present diffraction imaging experiment is as follows: for highly monochromatic X-rays, a perfect crystal has a limited angular acceptance (typically a few tens of microradians) in its diffraction plane, which in our geometry in Fig. 1 is the horizontal plane. But in the vertical plane, its angular acceptance is larger and can even exceed 1 mrad. This acceptance can be matched favourably with the characteristics of the waveguided beam, which is divergent (typically 1 mrad) in the vertical plane while maintaining its collimation in the horizontal plane. Strain sensitivity is then achieved with the collimated beam in the horizontal plane. High spatial resolution is utilized in the vertical direction, in which local structural variations at the sample are registered by projecting them, magnified, on a two-dimensional detector placed far from the sample. So spatial resolution and strain resolution are not correlated, as they are obtained in orthogonal directions: spatial resolution in the horizontal plane has to be sacrificed in order to obtain good strain sensitivity.

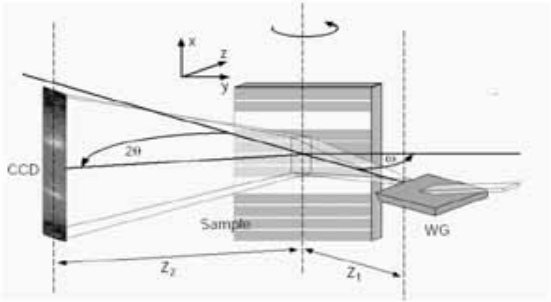

Figure 1 Diffraction imaging set-up. The beam arriving on the waveguide (WG) surface is spatially compressed by the waveguide in the vertical direction; the beam leaving the waveguide is vertically divergent. This latter beam, impinging on the sample surface at an incident angle ω, is diffracted in the horizontal plane towards the two-dimensional CCD detector positioned at a fixed scattering angle 2θ. The waveguide disperses the beam in the vertical plane providing at the CCD detector a magnification $M = (Z_1 + Z_2)/Z_1 - Z_2/Z_1$ for any structural variations occurring at the sample surface in this plane. Z_1 is the WG–sample distance, Z_2 is the sample–detector distance. In a Bragg scan only ω is varied.

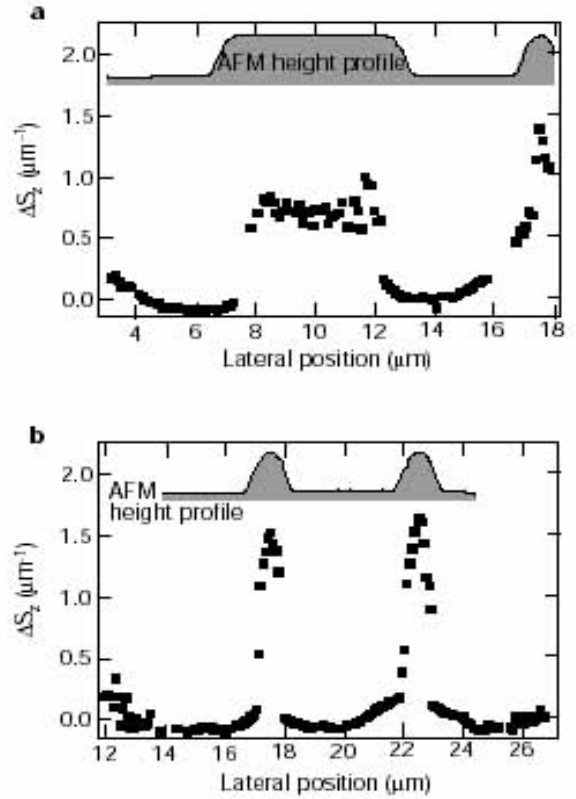

Figure 4 Spatial variation of strain under different oxidized stripes. The experimental data (symbols) indicate the position of the Si (004) Bragg peak in reciprocal space as a function of the lateral position on the sample. The data are presented as $\Delta S_z = S_z - S_{z_0}$, where S_{z_0} is defined in the text, and S_z refers either to the position of a fitted single peak or to the position of a detectable second peak. These peak positions are derived from fits of gaussian peaks (single or double) to the integrated $I(S_z)$ curves. The values of ΔS_z are presented for two zones of the sample corresponding to the wide SiO_2 stripe (**a**) and to two narrow sub-micrometre SiO_2 stripes (**b**). For comparison, the height profile of the sample as obtained by the scanning AFM measurements is shown as an inset at the top of each panel.

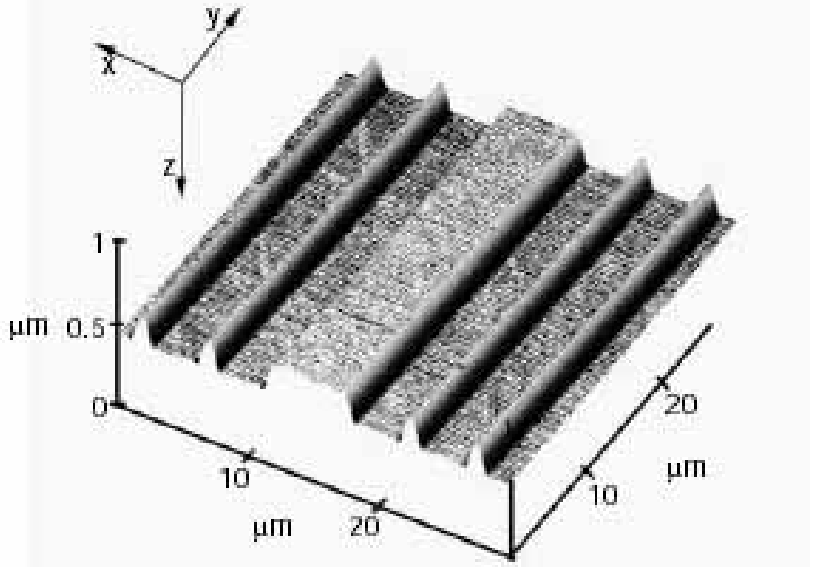

Figure 2 Atomic force microscopy scan of sample height profile. The SiO_2 stripes of different width extend ~ 170 nm above the sample surface.